Photocopy and Use Authorization

In presenting this dissertation in partial fulfillment of the requirements for an advanced degree at Idaho State University, I agree that the Library shall make it freely available for inspection. I further state that permission for extensive copying of my thesis for scholarly purposes may be granted by the Dean of the Graduate School, Dean of my academic division, or by the University Librarian. It is understood that any copying or publication of this thesis for financial gain shall not be allowed without my written permission.

Signature _____

Date_____

Investigation of Liver Transfer Rates in a Plutonium Biokinetic Model of the Rat - A Physiologically Based Pharmacokinetic Approach

by

Mark T Williams

A dissertation

submitted in partial fulfillment

of the requirements for the degree of

Doctor of Philosophy in the Department of

Nuclear Engineering and Health Physics

Idaho State University

July 2020

To the Graduate Faculty:

The members of the committee appointed to examine the dissertation of MARK T. WILLIAMS find it satisfactory and recommend that it be accepted.

Richard R. Brey, PhD
Major Advisor

Thomas F. Gesell, PhD
Committee Member

Chad L. Pope, PhD
Committee Member

Scott C. Miller, PhD
Committee Member

DeWayne R. Derryberry, PhD
Graduate Faculty Representative

Dedication

I dedicate my dissertation work to my family. A special thank you is offered to my wife, Sarah, for her enduring support of my professional efforts over the past 21 years. I also love and appreciate the support of my children who understood my goals and were patient with my pursuits. I have enjoyed support and encouragement from my parents, siblings, and close friends. The collective support from my family and friends contributed immeasurably to my success.

Acknowledgements

I wish to thank my committee members who were extremely generous with their time and expertise in support of my research efforts. I thoroughly enjoyed each of our professional interactions and I am invigorated by your enthusiasm for supporting student research. My research advisor, Dr. Richard Brey, deserves special recognition for his tireless efforts to support my research and his constant encouragement to push beyond my comfort level. I am grateful for his mentorship, friendship, and professionalism.

Table of Contents

List of Figures

List of Tables

Investigation of Liver Transfer Rates in a Plutonium Biokinetic Model of the Rat – A Physiologically Based Pharmacokinetic Approach

Dissertation Abstract – Idaho State University (2020)

Internal dosimetry models have been developed as a tool to estimate the physiological risks associated with the internalization of radionuclides. The models have progressively improved over time by simulating the results of animal studies and incorporating data collected from limited human exposures. The general approach to developing models is the collection of various tissue data from controlled tracer experiments and applying a set of first-order differential equations to the data. A compartmental representation, or compartmental model, is used to illustrate the relationship between the set of specific mathematical equations.

The focus of this research effort was to develop a physiologically informed, or physiologically based, model of the rat hepatic system for systemic exposure to plutonium. The model structure incorporates known anatomical, physiological and physiochemical behavior of plutonium in mammalian systems and supplements the model with proxy linear kinetics of endogenous and xenobiotic materials. The postulated system explicitly identified transferrin bound plutonium in blood plasma, Kupffer cells, and hepatocytes as the primary investigation compartments. The initial model included 22 physiologically informed fixed transfer rates and six adjustable transfer rates. All transfer rates to and from the plasma and within the liver were fixed *a priori* based on physiological assumptions. It was assumed plutonium-transferrin would behave similar to Dextran, a xenobiotic surrogate, while plutonium-citrate would behave similar to iron, an endogenous element. The initial model had a reported $\chi^2 = 6.86$ and 3.28 for the liver and

plasma systems respectively. The p-value statistic was reported as 0.55 for the liver and 0.9156 for the plasma. The initial model indicates that direct physiological kinetics in the rat hepatic system adequately describe the translocation of plutonium citrate between the liver and the vascular system for systemic exposure in rats. A secondary experiment was conducted to examine a limited effort to optimize two transfer parameters that underperformed in the initial model. The structure of the physiologically informed model permitted physiological interpretation of the optimized transfer rates and strengthened the confidence in the optimized parameters. The study supports the premise that physiologically informed *a priori* transfer rate estimates can be employed in an empirical modeling process.

Key Words: Plutonium, Internal Dosimetry, PBPK, biokinetic model, rat hepatic system, AIC.

1 Introduction

A computational methodology for describing the metabolic behavior of radioactive materials within the human body is essential for estimating radiation dose from occupational, environmental, or medical exposures. The behavior of radioactive material in mammalian systems has been studied extensively since the early days of the nuclear weapons programs. Concern regarding the retention, distribution, and excretion of internalized radionuclides was needed for protection of occupational workers and the public. Various mammalian species studies, limited human studies, and accident exposure studies were conducted in order to develop radionuclide specific biokinetic models (BK) capable of providing useful information regarding the behavior of radionuclides in the human body. The derived models have been successfully utilized to create public and occupational health exposure standards as outlined in the numerous International Committee on Radiation Protection (ICRP) and National Council on Radiation Protection (NCRP) documents. The models provide standardized, conservative estimates of radiation dose needed for administrative purposes; and they provide the dosimetry basis for the development of procedures needed to assess the magnitude of radionuclide intakes from post exposure bioassay data. Many of the current biokinetic models are expanded to address demographic (age and sex) differences in a general public exposure scenario. Additionally, the models have been increasingly used to justify and evaluate the effectiveness of medical interventions, specifically chelation therapy for actinide exposures.

1.1 Model Categories

1.1.1 Empirical and Semi-Empirical Models

The collection of ICRP BK models can generally be described as empirical, semi-empirical, or even semi-physiological. The models are developed primarily from animal studies and expanded when human exposure data is readily available. The structure of the model consists of homogeneous compartments interconnected by transfer pathways assumed to behave as linear 1st order kinetic transfer rates. The system is empirically solved to provide transfer rates that adequately describe measured excretion and organ retention data. Increased understanding of tissue specific accumulation and radiation exposure risk has led to the development of very complex models that identify relevant accumulation compartments which are often identified as a specific organ or part of an organ system.

The ICRP Publication 67 systemic model for Plutonium is a complex compartmental representation of an empirically solved model with physiological labels. One of the challenges of this type of modeling approach is the appearance of physiologically inconsistent transfer pathways that provide for mathematically improved empirical fitting at the expense of physiological relevance. Figure 1-1 depicts such an anomaly as seen in the direct transfer from “Other soft tissue compartment ST1” to “Urinary bladder contents” compartment. A revised model, Figure 1-2 below, has been proposed to correct this deficiency and update the number of compartments, transfer pathways, and transfer rates to reflect a more biologically consistent representation with improved empirical fits to an updated set of human exposure data.

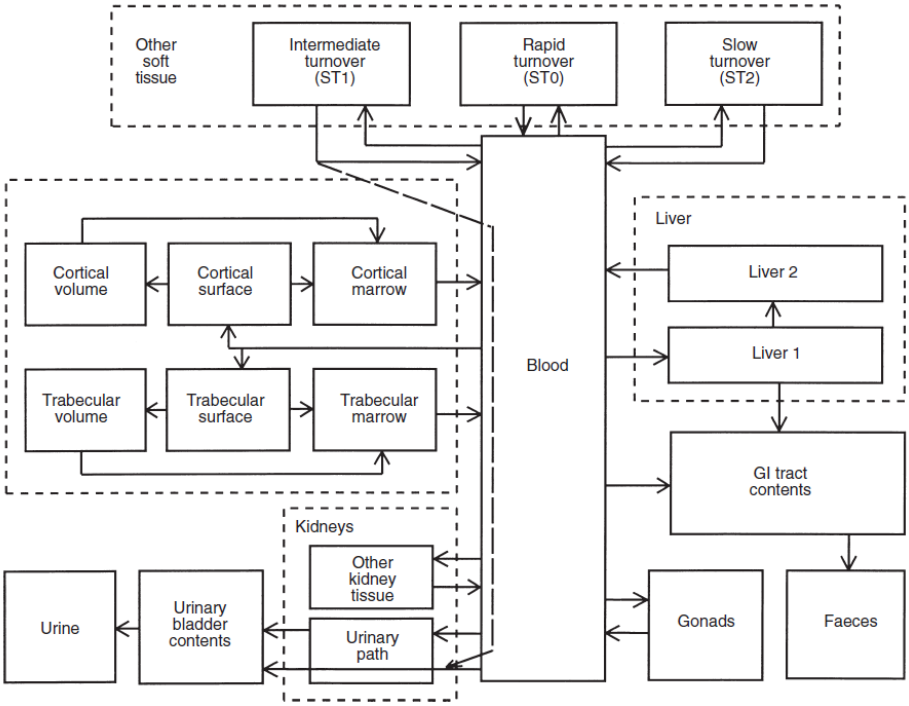

Figure 1-1 ICRP 67 Plutonium Systemic Model (Leggett, 2003)

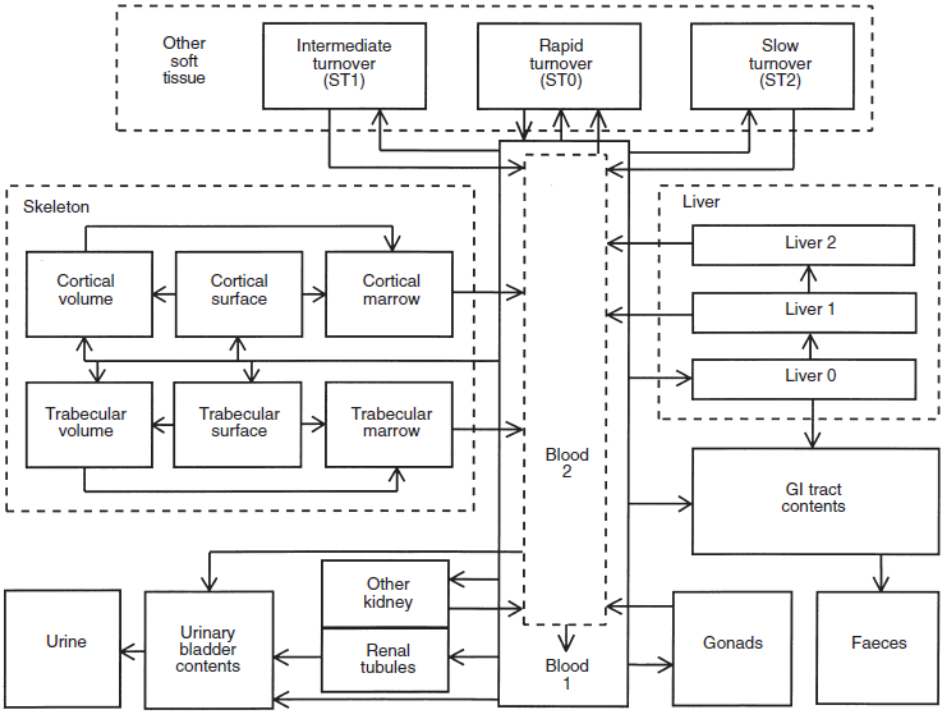

Figure 1-2 Proposed Updated Plutonium Systemic Model (Leggett, 2003)

Empirical compartment models are limited in their ability to extrapolate across varying exposure conditions and different clinical interventions as seen in attempts to update these models for chelation therapy for human plutonium exposures (Konzen, 2014).

1.1.2 Mechanistic Models - Physiologically Based Pharmacokinetic Models

Physiologically based pharmacokinetic models (PBPK) are a form of mechanistic model utilized heavily by the pharmaceutical industry to describe the absorption, distribution, metabolism, and elimination (ADME) of drugs in the preclinical phase of drug development. PBPK models incorporate physiochemical and biochemical information of the compound with anatomical and physiological parameters of the biological system to build a mechanistic framework. The framework can be utilized to integrate in-vitro data which can later be extrapolated to in-vivo observations based on the mechanistic understanding. The success of these models in pharmaceutical development has increased their use in environmental risk exposure assessments. The scope and complexity of the models, similar to empirical model development, is a function of the intended purpose of the model. However, a key advantage at any level of complexity is the ability for PBPK models to predict behavior of the compound for situations other than those directly measured in animal or human studies (U.S. Environmental Protection Agency (EPA), 2006).

A major limitation of mechanistic “bottom-up” model development is the incredibly large amount of information necessary to inform a complete model of the system. Parsimony is preferred due to limited data availability and to be in a position to defend the model assumptions. Therefore, PBPK model development is attained by

depicting routes of entry, storage organs, metabolism sites, elimination routes, explicit representation of target tissues, and lumping of non-target tissues with similar physiochemical behaviors (U.S. Environmental Protection Agency (EPA), 2006). Tissues are often represented with a unique set of physiological (i.e. blood flow) and physiochemical (i.e. partition coefficient) parameters.

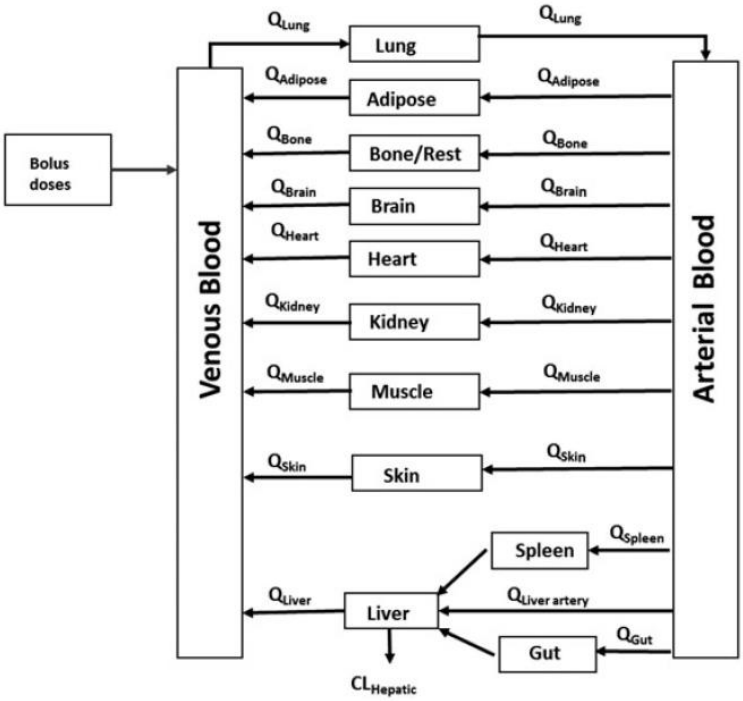

Figure 1-3 Generic PBPK model framework (Ye, Swati, & Korzekwa, 2016)

1.1.3 Hybrid Models

A recent effort to improve the predictive capability of the americium BK models for chelation therapy has been to incorporate a pharmacokinetic "front-end" to the traditional BK model structure, Figure 1-4 (Miller, et al., 2019). This approach involves the integration of a physiological delivery mechanism for material from the vascular space to the extra-cellular fluid space of the various organs before empirically solving for

the remaining transfer rate constants. The approach is similar to the front end of a generic PBPK model solution, but does not attempt to physiologically explain or identify the mechanistic transport rates beyond the vascular to ECF space. An interesting effect of this hybrid model is a new model for americium that is not comparable to the current ICRP BK models for americium. This distinct difference in number and type of compartments, as well as the stated value of transfer rates, reveals a weakness in identifying the physiological relevance of the transfer rates in these empirical models.

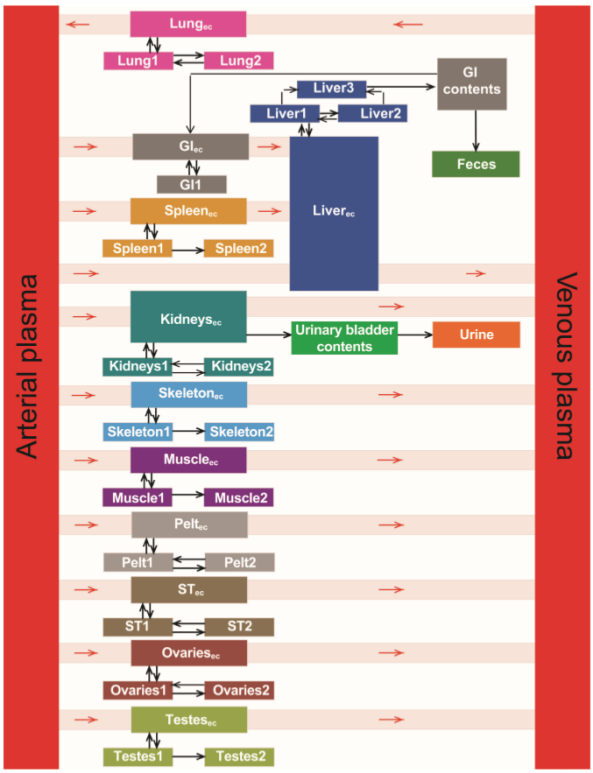

Figure 1-4 Americium systemic biokinetic model including pharmacokinetic front-end (Miller, et al., 2019)

1.2 Research Objectives

The primary objective of this research is to identify and model direct physiological kinetics for the transfer of plutonium between the liver and the vascular system in rats at an early time period, less than 48 hours, after systemic exposure to plutonium citrate (Pu-citrate). Direct physiological rates can be compared to empirically derived kinetic transfer rates to investigate the suitability of empirically derived transfer rates as surrogates for physiological transfer kinetics in an empirical model.

1.3 Hypothesis

H_O: Direct physiological kinetics in the rat hepatic system adequately describe the translocation of plutonium citrate between the liver and the vascular system for systemic exposure in rats.

H_A: Direct physiological kinetics in the rat hepatic system do not describe the translocation of plutonium citrate between the liver and the vascular system for systemic exposure in rats.

The model will be compared to the available rat necropsy data and the fit assessed using a chi-squared test statistic. A model fits these data when the chi-squared test statistic is small and the associated p-value is large. A model fails to fit the data when the chi-squared test statistic is large and the p-value is small.

2 Literature Review

2.1 Liver Physiology

The liver is a vital organ for maintaining the iron homeostasis of mammalian species. The liver is also responsible for glucose metabolism, hormone synthesis, infection control, and nutrient absorption from the small intestine. The liver receives approximately 80% of its blood from the portal vein and 20% from the hepatic artery in order to provide these important functions. Blood from the portal vein is mixed with oxygenated blood from the hepatic artery and the combined flow is circulated through the sinusoids. Sinusoids are lined with liver sinusoidal epithelial cells (LSEC) that provide a fenestrated barrier between blood and hepatocytes. LSEC account for 15-20% of total liver cells, but their elongated flat shape reduces their volume to less than 3% of total liver volume. The cells are the most permeable endothelial cells in the mammalian system and the fenestrate serve to remove very large particles (>150 nm) from the blood stream as well as maintain pressure and flow dynamics in the Space of Disse', located between LSEC and hepatocytes. The LSEC exhibit a very high rate of endocytic activity and strong lysosomal activity which aids in the removal of waste products from the blood (Poisson, et al., 2017).

2.1.1 Kupffer Cells

Kupffer cells are the primary macrophage system in the liver and these amoeboid-shaped cells colonize along the LSEC and can extend villi projections into the Space of Disse'. Kupffer cells account for up to 90% of total body macrophages and consume various particles via phagocytosis or pinocytosis. Kupffer cells are heterogeneously distributed throughout the sinusoids with increased concentration in the periportal

regions. The function, size, and fenestrate diameters of the cells are also heterogeneous and depends on their location in the liver. Cells in zone 1 have a higher phagocytic activity compared to counterparts in zone 3 likely due to the increased exposure to xenobiotic substances (Basit, Tan, & Webster, 2019). Kupffer cells play an important role in iron homeostasis through erythrophagocytosis of senescent red blood cells. The iron scavenged through this process is sequestered in ferritin and then released into the Space of Disse' or sinusoids for recapture by hepatocytes. Ferritin released from Kupffer cells average 2,400 iron atoms per molecule. (Sibille, Kondo, & Aisen, 1988). The population of Kupffer cells in the liver is constant, with a calculated life-span of 3.8 days, that is regulated through apoptosis (Naito, Hasegawa, Ebe, & Yamamoto, 2004). Some of the cells are phagocytized by neighboring Kupffer cells while others migrate to the periportal areas and hepatic lymph nodes before death (Basit, Tan, & Webster, 2019).

2.1.2 Hepatocytes

Hepatocytes, parenchymal cells, account for the vast majority of cells and largest cell volume of the liver. Their typical dimension is about 20 to 30 microns and they exhibit a life span of 200 to 400 days (MacDonald, 1961). These cells are capable of adjusting to continuously variable metabolic demands and therefore have the ability to absorb a large number of substrates and secrete endogenous metabolites and xenobiotics into the bile.

One of the essential functions of hepatocytes is to store iron, in the form of ferritin, and release the iron as homeostasis requires. There are several mechanisms involved in the transfer of iron from blood plasma. The transferrin receptors, TfR1 and TfR2, have been identified as the primary mechanism for transport of iron since 99% of all iron in

plasma is bound to transferrin. Secondly, several divalent membrane transporters have been identified, e.g. DMT1 and ZIP, as major transporters of non-transferrin bound iron (NTBI) (Ballatori, 2002). Ferritin receptors are another transporter that is highly expressed in hepatocytes and exhibits rapid transport mechanism. In vitro studies of isolated hepatocytes report rapid uptake of ferritin bound iron at the rate of 160,000 iron atoms per cell per minute and this rate is not impeded by the presence of iron-loaded transferrin (Sibille, Kondo, & Aisen, 1988). Ferritin is a ubiquitous protein, inter-cellularly located in the cell plasma, with the ability to bind divalent and trivalent metal ions with a capacity up to 4,500 g atoms of iron as Fe(III) (Joshi, Sczekan, & Fleming, 1989). Regardless of the non-transferrin receptor mechanism, in vitro studies of rat hepatocytes report highly efficient, 58% to 75%, hepatic first pass removal of low molecular weight NTBI and conclude that in vivo efficiency should be even greater (Brissot, Wright, Ma, & Weisiger, 1985).

2.1.3 Bile

Bile is made up of the bile acids, pigments, and other substances dissolved in an alkaline electrolyte solution (Barrett, Brooks, Boitano, & Barman, 2010). Rats do not have a gallbladder and therefore possess a continuous flow of bile from the hepatocytes to the duodenum. Many of the substances excreted in bile to the duodenum are actively absorbed in the small intestine and then excreted again by the liver in a process known as enterohepatic circulation. This process ensures optimal concentrations at the site of their physiological action and also provides a control mechanism in the homeostasis of trace elements like copper and iron (Kuipers, et al., 1985).

2.2 Plutonium Chemistry

Plutonium (Pu) is a radioactive element of the actinide family with multiple oxidation states, +3 to +7, and can often exist in multiple oxidation states simultaneously while in solution (ICRP, 1986). Plutonium was first synthesized by the bombardment of uranium with deuterons in 1940 and subsequently generated by transmutation of uranium in nuclear reactors on a large scale in modern times. The most common isotopes of plutonium are ^{238}Pu and ^{239}Pu and they are the most widely studied for potential health effects due to their use in industrial applications, electrical power generation, and nuclear weapons deployment (U.S. Department of Health and Human Services, 2010). The complex chemistry of Pu and its potential health effects were recognized early in its production and as such there was urgent need to understand its behavior in biological systems. By February 8, 1944 Berkeley Labs had acquired 11 mg of Pu from which to begin tracer studies in rats (Durbin, 1972).

2.3 Plutonium in-vivo

2.3.1 Systemic Absorption

In-vivo the mammalian physiological networks have no natural affinity to Pu as its existence in nature is extremely rare. Tetravalent Pu, Pu(IV), is strongly hydrolyzed at physiological pH (Allard, Kipatsi, & Liljenzin, 1980) which results in the formation of polymeric, colloidal products that are relatively insoluble (Durbin, Plutonium in Man: A new look at the old data, 1972). Systemic studies require the intravenous (i.v.) injection of Pu in a form that resists initial formation of in-situ polymerization so as to behave similarly to monomeric Pu introduced to the systemic circulation from inhalation, ingestion, or wound exposures. To this end, many systemic Pu studies utilize an injection

solution with Pu citrate acting as a solvent. Citrate is a naturally occurring cellular agent important in the metabolism of carbohydrates, proteins, and fats. It is produced in the mitochondria via the citric acid cycle (Schimmelpfeng, 2009). The introduction of a bolus of Pu citrate creates an initial blood plasma concentration such that the Pu citrate complex resists initial polymerization and allows dissociated monomeric Pu to interact directly in the blood plasma system. The monomeric Pu, free Pu, is competitively capable of binding to various plasma proteins, polymerize, or bind to unbound citrate. The binding of monomeric Pu to plasma proteins is rapid and greater than 95% of Pu is bound, predominantly to transferrin, within 48 hours of injection (Durbin, Horovitz, & Close, 1972; Jensen, et al., 2011). Pu will readily form complexes of similar stability as the trivalent transition metals; notably iron (Fe^{3+}) because of the metals' charge to radius ratios are similar (Jensen, et al., 2011). The chemical similarity of Pu^{4+} and Fe^{3+} at the systemic level is important with respect to the metal transport protein serum transferrin (Tf) and serum albumin to a much lesser extent.

Transferrin-Plutonium (Pu-Tf) binding affinity is well established. However, the confirmation of the binding sites on the transferrin C-terminal or N-terminal has not been elucidated until recently. Transferrin's role in serum plasma is to strongly bind two Fe^{3+} ions and transport the Fe to a diverse set of cellular networks for Fe use or storage. Transferrin is a bilobed, C-terminal and N-terminal, glycoprotien of approximately 80 kDa arranged in two homologous halves with an iron binding site located at the bottom of the inter-domain cleft in each lobe. The average speciation of iron-transferrin (Fe-Tr) binding configurations is 37% apo-Tf, 45% Fe_NTf, 8% Fe_CTf, and 11% Fe_2Tf (Jensen, et al., 2011) for normal blood iron loading concentrations. The relative abundance of free Tf

binding sites provides a surplus of competitive process binding between the Pu-Citrate and Pu-Tf interaction created by the experimental bolus injection. The first stability constants (log K_1) for Pu(IV)-Cit, Pu_N-Tr, and Pu_C-Tr, Table 2-1, indicate that monomeric Pu introduced to systemic circulation through other routes of entry (inhalation, wound, or ingestion) are likely to preferentially bind to the large number of free transferrin binding sites. Competitive binding of Pu-Tf, Pu-Citrate, and the systemic distribution by blood flow from plasma to various organs in systemic studies is an important nuance and is key to the physiological basis for tissue and cellular uptake mechanisms in the early time sequence. This phenomena is much less important at later time points when the majority of Pu is bound to transferrin.

Table 2-1 First stability constant binding affinity for Pu(IV) (Ansoborlo, et al., 2006)

	Pu(IV) Log K_1
Citrate	15.3
Transferrin (Tf)	22.5
Tf-C terminal	23.2
Tf-N terminal	21.9

2.3.2 Organ and Tissue Distribution

The translocation of material to various organs is primarily a function of vascular flow and the amount of material presented to each organ is a function of the time-dependent vascular concentration. Traditional compartmental models assume that compartments are well-stirred and have a uniform distribution of material within the tissue volume. This assumption permits a simplified approach for the transport of material leaving an organ or tissue structure. PBPK models similarly utilize a quasi-equilibrium assumption to calculate a blood to tissue partition coefficient to account for

the concentration of material leaving an organ. However, it is well understood that most tissue are not homogenous and distribution among various cell types is highly dependent on specialized functions of the cell and the anatomical structures of the individual tissue space. The translocation of Pu in the rat is predominantly divided among the plasma, liver, skeleton, and other soft tissues to a lesser extent. Multiple kinetic studies of rats from 1947 to 1968 confirm the deposition pattern summarized in Table 2-2.

Table 2-2 Distribution of i.v. injected ^{239}Pu(IV) citrate in young adult female Sprague-Dawley rat (Durbin, Horovitz, & Close, 1972)

	Pu content (% of injected activity)			
Time (hr)	Plasma	Skeleton	Liver	Soft tissues + extra cellular fluid
0.125	52.5	4.2	3.4	39.8
0.25	45.6	5.6	5.5	41.5
0.5	41.5	7.1	7.9	41.6
1	38.0	11.2	9.1	39.6
2	33.9	13.8	11.4	38.0
6	27.1	25.8	15.9	27.5
12	17.4	37.8	18.2	20.8
24	6.1	51.9	22.7	13.8
48	1.8	54.5	23.1	-

The early pattern of distribution from Pu-Citrate studies is utilized in empirical BK models to define the behavior of monomeric plutonium without regard for the influence of Pu-Citrate on the deposition pattern. Each organ system has unique and complex deposition and retention patterns. The details of these patterns, while important, are off topic to this particular review. Therefore, the focus will be on the translocation from plasma and deposition within the liver.

Monomeric plutonium is generally believed to be deposited within the liver hepatocyte cells while polymeric plutonium is associated with the Kupffer cells or other

cells in the sinusoidal lining of the liver (Grube, Stevens, & Atherton, 1978). The well-established association of Pu with transferrin was not considered a precursor condition for deposition within hepatocytes and it was recognized that other mechanisms of intracellular transport were also responsible for the deposition within hepatocytes (Durbin, Horovitz, & Close, 1972). Jensen et al. (2012) more recently identified that the only form of Pu-Tr that readily infiltrated mammalian cells, utilizing the transferrin-transferrin receptor iron uptake pathway, was the specific plutonium-iron-transferrin complex of Pu bound to the C-terminal and Fe bound to the N-terminal (Pu_CFe_NTf). Identification of this intracellular pathway highlights a unique condition where Pu is only able to marginally access the transferrin mediated iron uptake pathway, therefore Pu must utilize other pathways in order to be retained by the liver.

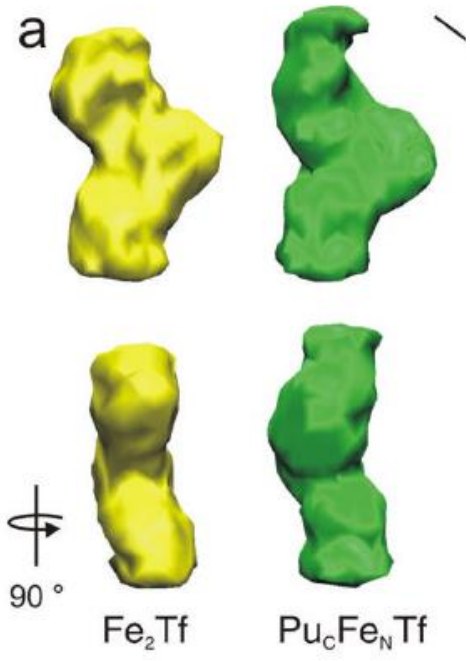

Figure 2-1 Geometric similarity between Fe_2Tf and Pu_CFe_NTf (Jensen, et al., 2011)

Early studies of monomeric plutonium kinetics identified a close similarity between the half-time of the first exponential term for the removal of Pu-citrate, 0.97 hours, and the half-time for the removal of ^{59}Fe, 0.93 hours (Turner & Taylor, 1968). The transport of the Pu-citrate, or Pu bound to other lower molecular weight plasma constituents, therefore is significant in the early phases of systemic studies.

Polymeric Pu, also referred to as colloidal or aggregated, is predominantly retained within the reticuloendothelial system, which include Kupffer cells in the liver. Cross species studies of mice, rats, and canine consistently highlight the increased liver uptake and retention of polymeric vs monomeric Pu exposures (Turner & Taylor, 1968). The increased uptake in the liver corresponds to increased rates of depletion of Pu from the plasma due principally to the effectiveness of the liver in removing colloidal particles. Recent x-ray fluorescence (XRF) studies of a cell line derived from pheochromocytoma of the rat adrenal gland (PC12) exhibit both transferrin and non-transferrin mediated uptake of Pu. The *in vitro* study of PC12 cells reinforces the concept of non-transferrin mediated cellular uptake of Pu-citrate, but it also displayed transcellular transport of *in situ* formed Pu polymer by non-phagocytic cells (Aryal, et al., 2011). Furthermore, this study reinforces the association between Fe and Pu in the uptake and distribution within cells.

2.3.3 Excretion

Physiological removal of Pu-citrate is accomplished via urinary and fecal excretion, Figure 2-2. The ratio of fecal to urinary excretion at 24 hours post injection is reported as 3:1; while the ratio at 30 days increases to 17:1 (Carritt, et al., 1947). The increase in the ratio is likely a function of the reduction in Pu urinary excretion as the Pu-

citrate is degraded and transformed into Pu-Tr; which is non-dialyzable by the kidney (Popplewell, Stradling, & Ham, 1975).

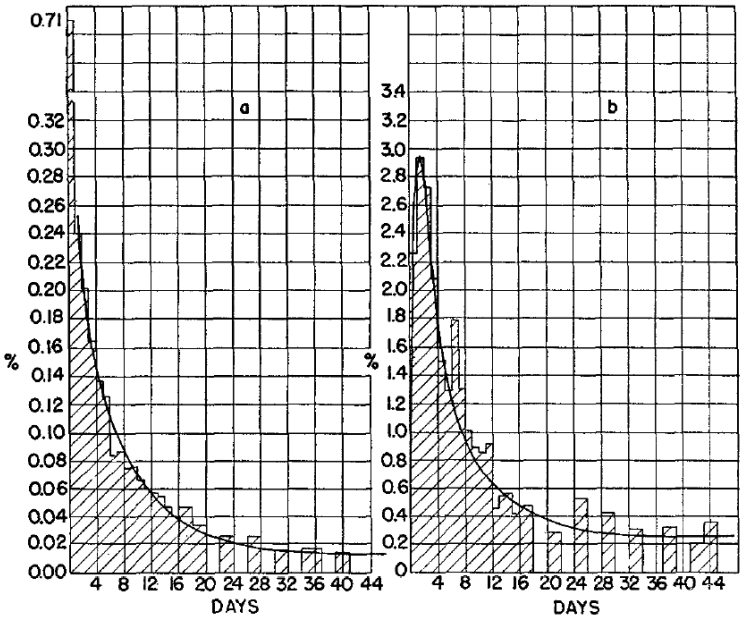

Figure 2-2 Percent of dose excreted per day. Urinary (a) and fecal (b) excretion of plutonium following i.v. administration of Pu(IV) citrate. (Carritt, et al., 1947)

Fecal excretion of Pu is directly correlated to the loss of Pu from the liver. Cannulated main bile duct and small intestine perfusion studies of the rat, Figure 2-3, report that bile excretion into the duodenum as a major constituent of Pu in the intestinal track. However, appearance of Pu in the remaining segmented intestinal zones indicates that bile excretion is not the only mechanism of Pu loss to the intestine (Ballou & Hess, 1972). Presence of Pu in the bile and its deposition into the duodenum does not account for the physiological process of enterohepatic recirculation of material and Ballou and Hess made no attempt to measure the re-absorption of Pu along the small intestine.

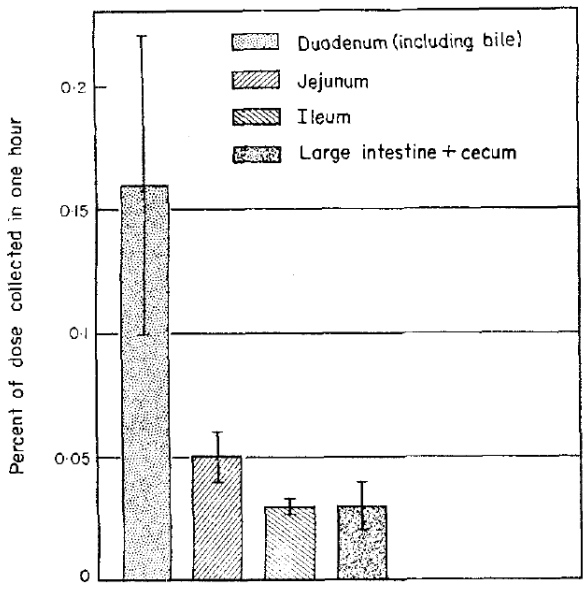

Figure 2-3 Plutonium excretion into perfused gut segments (average +/- SD) from 3 rats for the first hour after i.v. administration of Pu-citrate. (Ballou & Hess, 1972)

2.4 Rodent - Plutonium Biokinetic Models

Published biokinetic models (BK) of the rat are sparse since the focus of these early rat studies was to observe Pu behavior in vivo and compare the data to other species. Ultimately the goal at the time was to develop a BK model for human exposure scenarios. Two models were proposed by the same author to illustrate the kinetics of Pu-citrate in rats and mice. The first model developed for the rat, see Figure 2-4, illustrates the knowledge of Pu in vivo behavior from 0.25 to 18 hours post i.v. injection of Pu(IV)-citrate (Durbin, Horovitz, & Close, 1972).

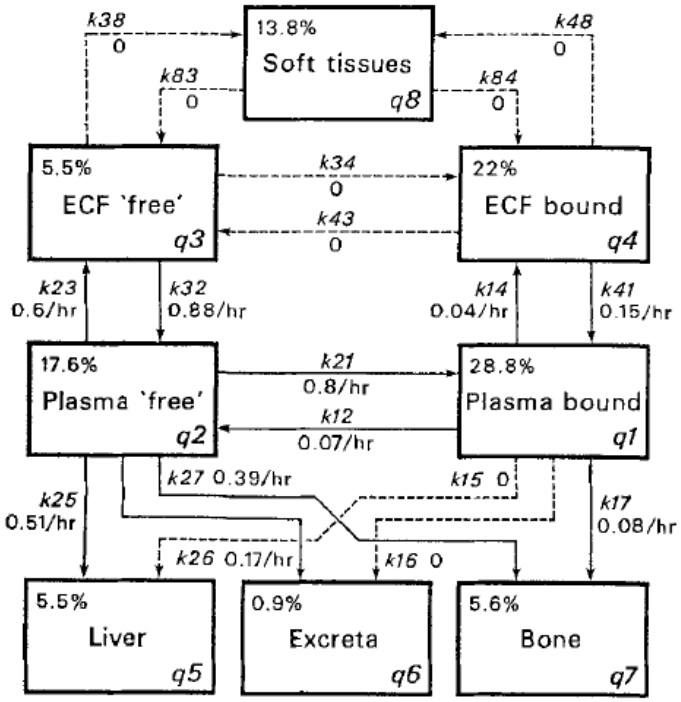

Figure 2-4 Biokinetic (BK) model of Pu transport and uptake in tissues of the rat 0.25-18 hr after i.v. injection of ^{239}Pu(IV) citrate (Durbin, Horovitz, & Close, 1972).

The model provided a focused examination on the division of Pu in the plasma either bound to transferrin or un-bound from transferrin and the fate of the two different forms. The 'free' Pu, which was likely still bound to citrate at these early time points, was distributed between the extra-cellular fluid (ECF) space, liver, bone, and excreta. The bound fraction, was distributed between the ECF space, liver, bone, and excreta in the same manner as the unbound material. The inter-compartmental transfer rates were empirically derived from the data observed in Table 2-2. Limitations in the quality and specificity of the data prevented the author from solving all transfer rates depicted in the model and therefore many of the rates were fixed at a value of zero. Additionally, it was not possible to describe the very early kinetics occurring before 15 minutes and the model

only reflects events after 0.25 hours. The system also did not attempt to model recycling from the intestine or bone and as such the maximum time association for the model is 18 hours (Durbin, Horovitz, & Close, 1972).

The second model was developed in order to provide an improved explanation for the translocation of Pu between the plasma and ECF, referred to as interstitial water (I) in this study. The model was developed specifically for the mouse, but the author directly states that "interstitial water is a major circulatory compartment for iv-injected Pu(IV) citrate in small laboratory animals" (Durbin, Kullgren, & Schmidt, 1972). The simple model, Figure 2-5, indicates that diffusion of Pu-citrate, not bound to transferrin, is rapidly transferred from plasma (P) to I and is eventually returned to plasma. After 120 minutes in the mouse both P and I are cleared of plutonium at about the same rate. Durbin et. al, 1972 conclude that early circulatory kinetics of i.v. injected Pu-citrate in human, dog, rat, and mouse are similar because they have a common chemical basis; competition for Pu(IV) ions in the plasma between citrate and transferrin and between citrate and/or transferrin tissue ligands at the surface of hepatocytes and bone (Durbin, Kullgren, & Schmidt, 1972). In early time periods after systemic exposure the small plasma volumes and fast circulation times of rodents will inhibit plasma transferrin reactions in the injection bolus and lead to increased amounts of non-transferrin bound Pu being presented to the interstitial water, filtered through kidneys, and deposited in target tissues (Popplewell, Stradling, & Ham, 1975). Observations of the plasma plutonium curves for multiple species indicate that initial organ deposition is complete when Pu in plasma is less than 1% of injected activity, and for the rat this equates to approximately two days.

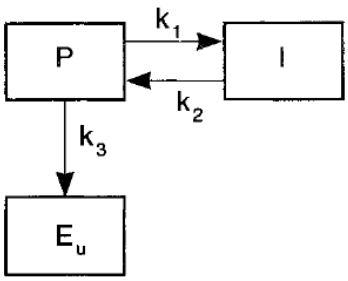

Figure 2-5 Tracer exchange in a two-compartment system between plasma (P) and interstitial water (I) with urinary excretion (E_u) for i.v. injection (Durbin, Kullgren, & Schmidt, 1972)

2.5 Physiologically-Based Plutonium Models

The majority of Pu models in the literature base the biokinetic parameters on sophisticated mathematical techniques and the resulting models often fail to provide sufficient physiological relevance. The quality of the model is a direct reflection of its intended use and the accuracy of its assumptions. Schimmelpfeng, 2009 proposed a physiological-based Pu compartment model structure based on conclusion by analogy of an aluminum model. Mammalian systems show similarities between the in vivo behavior of Pu(IV), Fe(III), and Al(III) and the author suggests that transport rates between compartments might be similar. The model, Figure 2-6, is not specific to the rat; but instead focuses on the mechanistic behavior of plutonium binding between transferrin and citrate and its subsequent distribution to target tissues and organs.

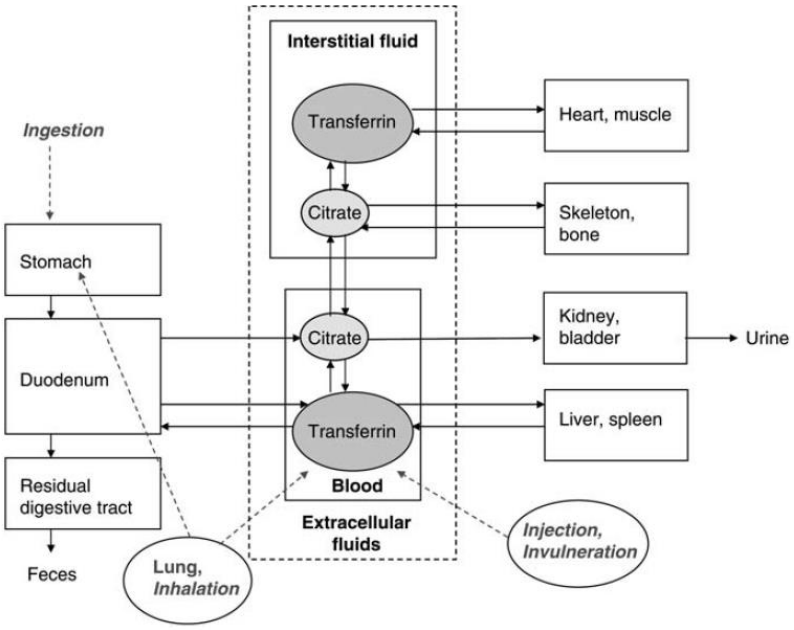

Figure 2-6 Basic physiological-based compartment model for the biokinetics of plutonium. Invulneration references exposure via a wound. (Schimmelpfeng, 2009)

The author did not attempt a solution to the model, but instead focused on similarities and differences between this model and the ICRP 67 BK model. The model provides a direct physiological relationship to the compartment transfer rates and thus an improvement in highlighting the mechanistic rationale underlying the rates.

2.6 Physiological data

2.6.1 In Vivo functional imaging of hepatic transport

Reif et al. 2017 utilized a two-photon microscopy-based system to image an intact segment of liver during the uptake and elimination of endogenous and xenobiotic molecules in the mouse. The imaging technique provides a rare glimpse into a relatively undisturbed in vivo system and allows for the quantification of the movement of fluorescent dextran, for endocytic transport, and cholyl-lysyl-fluorescein (CLF) for bile acid transport.

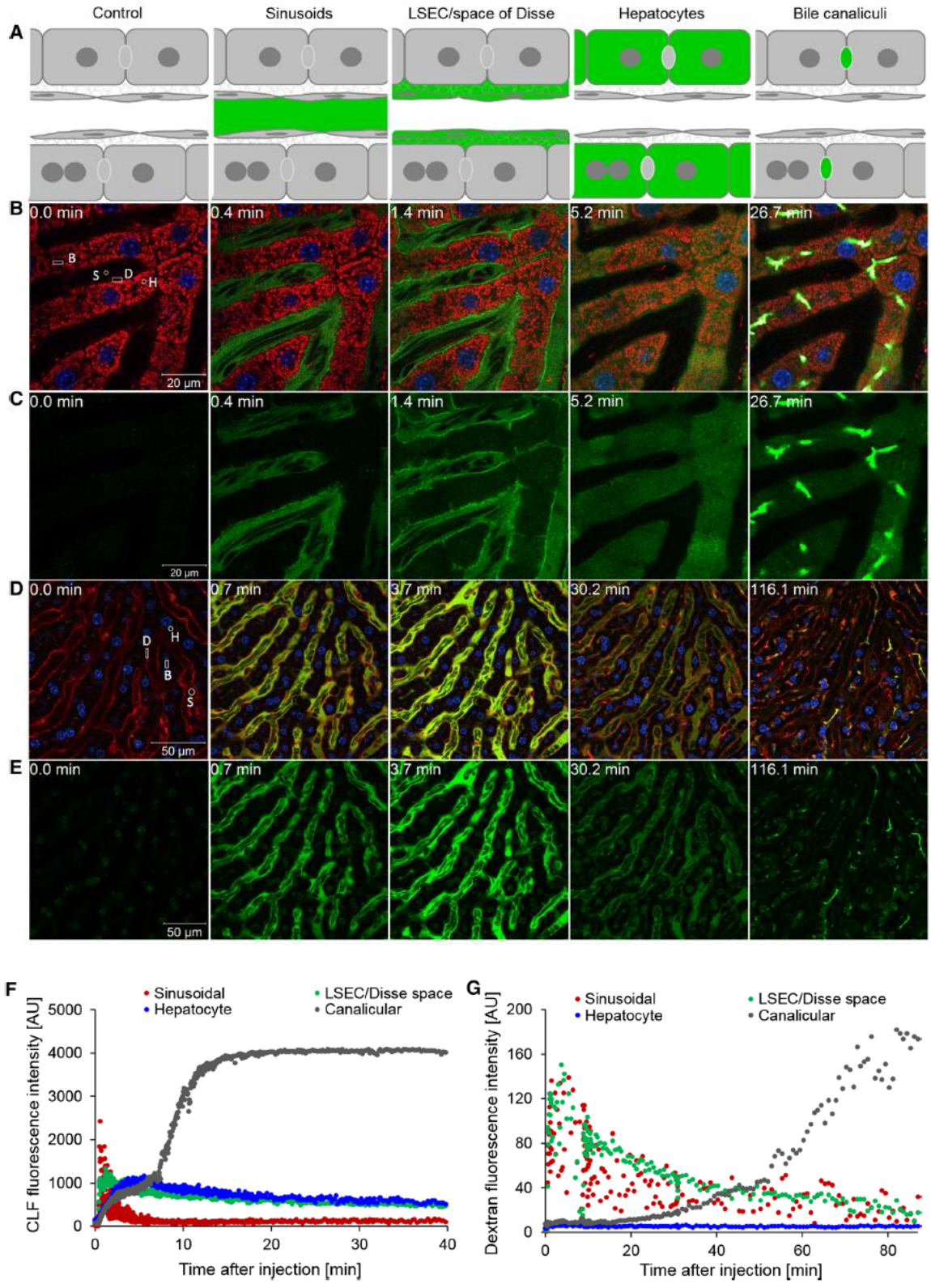

Figure 2-7 Hepatic transport of CLF and dextran (Reif, et al., 2017).

a) Illustration of the four stages during hepatic transport, namely appearance in the sinusoids, enrichment in the LSEC/Dissé space, uptake by the hepatocytes and transport into the bile canaliculi. b) Stills representing the four stages after CLF injection Hepatic morphology was visualized by injection of TMRE (red) and transport of CLF was followed (green). c) CLF channel only. d) Stills representing the four stages after fluorescent dextran 10,000 MW injection. Hepatic morphology is evident by the expression of membrane-targeted tomato (red) and transport of dextran was followed (green). e) Dextran channel only. Quantification of the CLF (f) and dextran (g) kinetics in the sinusoidal blood (S), LSEC/Dissé space (D), hepatocytes (H) and bile canaliculi (BC). Positions of quantification are indicated by white circles and rectangles in the left panels of b) and d).

Following i.v. injection of 2.5 mg/kg CLF the following hepatic transport imaging was obtained: 1) CLF appears in the sinusoids within approximately 15 seconds after tail vein injection and is rapidly cleared from the sinusoids, 2) the CLF is enriched in the LSEC/Space of Disse, 3) within 5 minutes the maximum homogenous signal in the cytosol of hepatocytes was observed and 4) rapid export into bile canaliculi. Injection of dextran, molecular weight of 10 kDa, exhibited very different kinetics. Dextran was visible in the sinusoids within 15 seconds after tail vein injection, but there was no concentration in the LSEC/Space of Disse. After approximately 15 minutes the dextran was detectable in the bile canaliculi and the intensity increased throughout the study time. Dextran remained circulating in the sinusoids five time longer than CLF. The calculated half-life for CLF and dextran are indicated in Table 2-3.

Table 2-3 Pharmacokinetic parameters obtained from in-vivo imaging

Compartment	**Half-life for CLF (min)**	**Half-life for dextran (min)**
Sinusoids	1.89	15.91
LSEC/Disse Space	13.46	19.15
Hepatocytes	34.17	not detectable due to transport in vesicles
Bile canaliculi	No detected decrease in fluorescence	No detected decrease in fluorescence

2.6.2 Enterohepatic transport of ^{59}Fe / Basolateral transfer

The homeostasis of iron is controlled through a regulated process of loss and reabsorption. Specifically, the loss of iron must be replaced by intestinal absorption. The kinetics of the basolateral transfer of iron across the duodenum was studied in both iron-adequate and iron-deficient rats. Duodenal segments were luminally perfused ex vivo and the mobilization of ^{59}Fe from the duodenal tissue into the absorbate was evaluated. Tissue to absorbate transfer increased in proportion to the mobilizable fraction or recently absorbed iron in the tissue, which is indicative of simple diffusion or carrier-mediated transport below saturation. The rate constant for mobilization from the segments into the absorbate for iron-adequate segments was reported as 0.0219 +/- 0.0046 min^{-1} (Schumann, Elsenhans, & Forth, 1999). The results from the previous study seem to be in agreement with a more recent study of the iron induced movement of the divalent metal transporter 1 (DMT1) and ferroportin (FPN) which are implicated in the import and export of Fe in enterocytes. The reported endocytosis time for DMT1 and FPN were each reported as 30 to 60 minutes (Nunez, 2010).

2.6.3 Translocation of transferrin from blood to bile

Transferrin is transferred both passively and actively from blood to bile. The active mechanism is regarded as the transferrin-transferrin receptor pathway when Fe is bound as either Fe_2Tf or iron bound the C-terminal (Fe_CTf). In rats that received differic rat transferrin (Fe_2Tf), 0.103% +/- 0.026% of the labeled Fe was excreted with bile within 3 hours and the corresponding transport rate was reported as $7.95x10^{-3}$ +/- $2.95x10^{-3}$ min^{-1}. Co-administered iron-free transferrin (apo-transferrin) was present in the bile at relatively stable concentrations with a passive transport rate of $1.01x10^{-3}$ +/- $4.05x10^{-3}$

min^{-1}. An interesting conclusion from this study is that Fe_2Tf is translocated to the bile both passively and actively. Additionally, 8% to 15% of biliary ^{59}Fe was not bound to transferrin (Regoeczi & Chindemi, 1995).

2.6.4 Non-transferrin bound iron (NTBI) kinetics

It has already been reported above that liver is very efficient at absorbing NTBI. Studies of both ferric and ferrous iron indicate a similar pattern of saturation kinetics, Table 2-4, and suggest a membrane carrier system may be involved in the uptake across hepatocytes. However, the study is not able to rule out the possibility of a rate-limiting step produced by the incorporation of iron into ferritin (Brissot, Wright, Ma, & Weisiger, 1985).

Table 2-4 Uptake of non-transferrin bound iron (NTBI) by perfused rat liver (Brissot, Wright, Ma, & Weisiger, 1985)

	Extraction (%)	**Km (μM)**	**Vmax ($nmol \cdot min^{-1} \cdot g\ liver^{-1}$)**
Ferrous Iron (Fe^{2+})	63 ± 4	22 ± 5	38 ± 7
Ferric Iron (Fe^{3+})	55 ± 2	14 ± 2	24 ± 2

2.6.5 Blood distribution transfer rates

Miller et. al 2019 describe the mechanistic parameters associated with the vascular movement of blood in a rat biokinetic system. Material introduced to the systemic circulation is initially translocated throughout the rat body with the vascular flow. The pharmacokinetic front-end, physiologically defined as the mass balance of blood flow, is defined in for a variety of rat tissues, Table 2-5. The data set used in the current effort has only plasma, skeleton, soft tissue/ECF, liver, and excreta; therefore, conservation of mass to these organs was maintained in the lumping routine.

Additionally, due to the creation of two plasma compartments, equal weighting was given to flow from each plasma compartment to maintain this mass balance.

Table 2-5 Blood distribution transfer rates in the rat (Miller, et al., 2019)

Source compartment[a]	Volume of source compartment (ml)	Target compartment[a]	Flow rate (L/h)	Transfer rate (day^{-1})[b]
vPlasma	4.95	$Lung_{ec}$	1.553	7,533
aPlasma	2.62	GI_{ec}	0.374	3,429
aPlasma	2.62	$Spleen_{ec}$	0.017	157
aPlasma	2.62	$Liver_{ec}$	0.064	583
aPlasma	2.62	$Kidney_{ec}$	0.354	3,244
aPlasma	2.62	$Muscle_{ec}$	0.351	3,216
aPlasma	2.62	$Skeleton_{ec}$	0.05	455
aPlasma	2.62	$Pelt_{ec}$	0.141	1,295
aPlasma	2.62	ST_{ec}	0.182	1,665
aPlasma	2.62	$Gonad_{ec}$	0.008	71
$Lung_{ec}$	0.34	aPlasma	1.553	109,448
GI_{ec}	2.04	$Liver_{ec}$	0.374	4,396
$Spleen_{ec}$	0.02	$Liver_{ec}$	0.017	27,088
$Liver_{ec}$	1.14	vPlasma	0.455	9,620
$Kidney_{ec}$	0.53	vPlasma	0.354	16,042
$Muscle_{ec}$	10.6	vPlasma	0.351	795
$Skeleton_{ec}$	5.22	vPlasma	0.05	228
$Pelt_{ec}$	17.64	vPlasma	0.141	192
ST_{ec}	15.46	vPlasma	0.182	282
$Gonad_{ec}$	0.59	vPlasma	0.008	318

[a] The prefixes "a" and "v" refer to arterial and venous, respectively. The subscript "ec" refers to extracellular.

[b] Transfer rate (day^{-1}) is given by flow rate (l/h) × 24/(volume of source (ml)/1,000).

3 Methodology

A full physiologically based pharmacokinetic model describing all mechanistic behaviors of in vivo Pu is not possible at this time due a lack of fundamental data required to build-up a comprehensive PBPK model. Instead, the modeling approach will focus on developing a BK model structure based on physiologically identifiable transport pathways with constant transfer rates. Specifically, this approach may highlight those pathways that dominate transport kinetics. The rates for known physiological functions will be applied based on specific measurements of Pu, Fe, or other endogenous substances in the body. Transfer rates without physiological data will be empirically solved based on the best fit to excretion and organ necropsy data. In order to substantiate this model structure the following assumptions are recognized:

1. Plutonium systemic exposures, i.v. injection of Pu-citrate, is distributed grossly between blood plasma, liver, bone, and soft tissues dominated by the ECF space.

2. Plutonium can exist in oxidation states +3 to +7, but at in vivo mammalian pH the preeminent state is +4.

3. Pu(IV) has similar physiochemical properties of Fe(III) and therefore will behave similarly when competing for transferrin binding sites and non-specific cellular metal transporters.

4. Plutonium not bound to transferrin will be bound to citrate or other low molecular weight blood proteins.

3.1 Model Structure

The basic premise for model development was to design an informative systems-based model that can be used to explore the utility of adopting physiological parameters,

a priori, instead of empirically derived parameters. The model structure utilizes *in vivo* and *in vitro* knowledge of Pu(IV) citrate behavior to define the main compartments needs for exploration of the premise with a specific focus on translocation to the liver.

The blood plasma is separated into two compartments; one represents the initial bolus of Pu(IV)-citrate while the other compartment represents the strong affinity of Pu(IV) and transferrin. The transfer rate between the two plasma compartments is a one-way fixed value representative of the amount material bound to transferrin within 48 hours post injection. Translocation of material away from the Pu-citrate plasma compartment is directed towards each of the organ systems via the pharmacokinetic front-end rates listed in Table 2-5. The only organ system with the possible return of Pu-citrate to plasma is the soft tissue ECF compartment; due primarily to the rapid exchange of blood between this lumped tissue compartment. All other organ systems are assumed to delay the Pu-citrate long enough for cellular influx or Pu dissociation and subsequent binding to transferrin. Pu-citrate transferred to the liver is maintained initially in the liver extra-cellular compartment which is indicative of the rapid blood flow between the vascular system and liver. Pu-Tf in plasma is transferred to and from each of the major organ systems using the pharmacokinetic front-end rates; with an explicit liver extra cellular compartment for Pu-Tf.

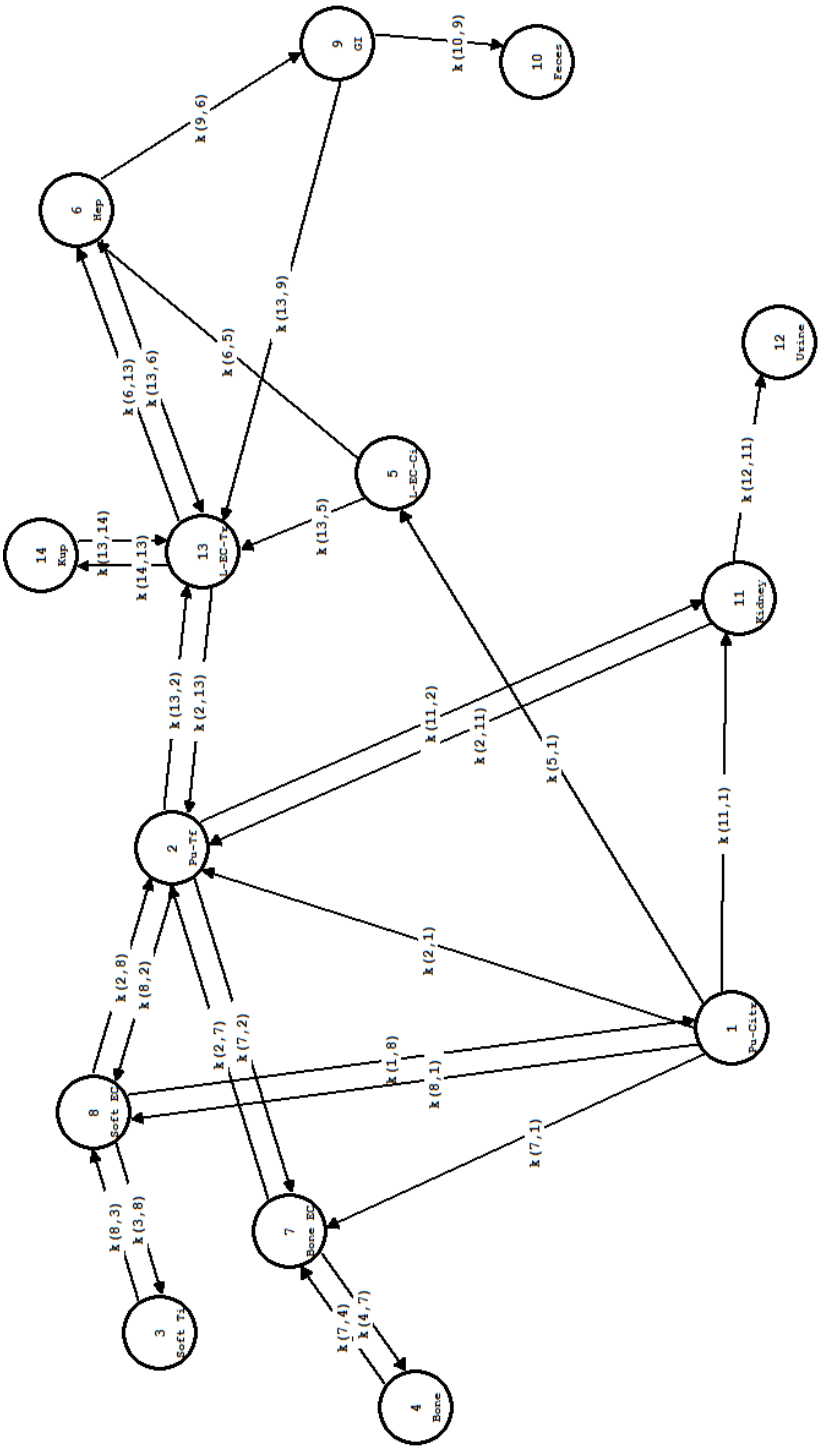

Figure 3-1 Proposed Biokinetic Model Structure

Table 3-1 Initial Model Compartment Identification Matrix

Parameter ID	Parameter ID
1 – Pu-citrate (Plasma)	8 – Soft Tissue
2 – Pu-Tf (Plasma)	9 – GI
3 – Soft Tissue	10 – Fecal Excretion
4 – Bone	11 – Kidney ECF
5 – Liver ECF – Pu-Citrate	12 – Urinary Excretion
6 – Hepatocytes	ECF 13 – Liver ECF – PuTr
7 – Bone ECF	14 – Kupffer Cells

Movement of Pu-citrate from the liver extracellular space is a one-way path to the Pu-Tf liver extra cellular space with a transfer kinetic equal to the rate of binding between the blood plasma compartments. An additional one-way pathway from the liver Pu-citrate compartment to hepatocytes also is depicted. This path is representative of the highly efficient first pass capture of non-transferrin bound iron in the liver. The hepatocytes can efflux Pu back to the liver extra cellular space, where it is assumed to rapidly bind with transferrin. An additional efflux pathway from hepatocytes to the gastrointestinal tract (GI) via biliary excretion is explicitly depicted. Pu-Tf in the liver extra cellular can access hepatocytes, via the transferrin-transferrin receptor, and also can access Kupffer cells. Kupffer cells are assumed to return Pu to the liver extra cellular space with rapid binding to transferrin again.

Hepatocytes efflux material via the biliary pathway and it is captured in the duodenum and assumed to either move along the GI or be reabsorbed into the hepatic vascular system across enterocytes. The movement of material across this path is

representative of the enterohepatic circulation responsible for the tight homeostatic control of Fe. Material from the GI tract is also excreted as feces.

Pu-Tf and Pu-citrate in plasma is directed toward the kidney extra cellular space for filtering via the glomerulus or active transport and reabsorption. No attempt is made to further delineate pathways to urine and the transfer rate is empirically resolved from excreta bioassay data. The soft tissue and skeleton are also empirically solved from their respective extra cellular compartments.

3.2 Modeling Software

The biokinetic software Simulation, Analysis, and Modeling II (SAAM II) was employed to solve the system of first-order, ordinary (linear) differential equations defined by the model structure in Figure 3-1. The iterative solving routine attempts to minimize the objective function, essentially the maximum-likelihood estimator, for the data set. Due to the large number of fixed parameters, the solving routine most notably attempts to solve the parameters associated with the necropsy data after passing through the fixed transfer rate parameters. The model is designed to explore the transfer of material through the liver and little effort will be utilized to improve fits associated purely with the empirically fitted parameters.

Table 3-2 Initial Model - Parameter estimates

	Source Compartment	Target Compartment	Transfer Rate ID	Transfer Rate (hr^{-1})	Reference	Fixed/ Fitted
1	Soft Tissue ECF	Pu-Citrate (Plasma)	k(1,8)	190	Table 2.5	Fixed
2	Pu-Citrate (Plasma)	Pu-Tf (Plasma)	k(2,1)	$1.069 \cdot 10^{-3}$	(Durbin, Horovitz, & Close, 1972)	Fixed
3	Bone ECF	Pu-Tf (Plasma)	k(2,7)	9.5	Table 2.5	Fixed
4	Soft Tissue ECF	Pu-Tf (Plasma)	k(2,8)	190	Table 2.5	Fixed
5	Kidney ECF	Pu-Tf (Plasma)	k(2,11)	668.4166	Table 2.5	Fixed
6	Liver ECF-Pu-Tr	Pu-Tf (Plasma)	k(2,13)	15,295.5	Table 2.5	Fixed
7	Soft Tissue ECF	Soft tissue	k(3,8)	Adjustable	-	Fitted
8	Bone ECF	Bone	k(4,7)	Adjustable	-	Fitted
9	Pu-Citrate (Plasma)	Liver ECF-Pu-Citrate	k(5,1)	15.4166	Table 2.5	Fixed
10	Liver ECF-Pu-Citrate	Hepatocytes	k(6,5)	72.1	(Brissot, Wright, Ma, & Weisiger, 1985) (Fagerholm, 2009)	Fixed
11	Liver ECF-Pu-Tr	Hepatocytes	k(6,13)	1.217	(Reif, et al., 2017)	Fixed
12	Pu-Citrate (Plasma)	Bone ECF	k(7,1)	9.4792	Table 2.5	Fixed
13	Pu-Tf (Plasma)	Bone ECF	k(7,2)	9.4792	Table 2.5	Fixed
14	Bone	Bone ECF	k(7,4)	Adjustable	-	Fitted
15	Pu-Citrate (Plasma)	Soft Tissue ECF	k(8,1)	130.146	Table 2.5	Fixed
16	Pu-Tf (Plasma)	Soft Tissue ECF	k(8.2)	130.146	Table 2.5	Fixed
17	Soft Tissue	Soft Tissue ECF	k(8,3)	Adjustable	-	Fitted
18	Hepatocytes	GI	k(9,6)	1.897	(Ballou & Hess, 1972)	Fixed
19	GI	Feces	k(10,9)	Adjustable		Fitted
20	Pu-Citrate (Plasma)	Kidney ECF	k(11,1)	67.5833	Table 2.5	Fixed
21	Pu-Tf (Plasma)	Kidney ECF	k(11,2)	67.5833	Table 2.5	Fixed
22	Kidney ECF	Urine	k(12,11)	Adjustable	-	Fitted
23	Pu-Tf (Plasma)	Liver ECF-Pu-Tr	k(13,2)	15.4166	Table 2.5	Fixed
24	Liver ECF-Pu-Citrate	Liver ECF-Pu-Tr	k(13,5)	$1.069 \cdot 10^{-3}$	(Durbin, Horovitz, & Close, 1972)	Fixed
25	Hepatocytes	Liver ECF-Pu-Tr	k(13,6)	$2.083 \cdot 10^{-3}$	(MacDonald, 1961)	Fixed
26	GI	Liver ECF-Pu-Tr	k(13,9)	183.1666	Table 2.5	Fixed
27	Kupffer Cells	Liver ECF-Pu-Tr	k(13,14)	$1.096 \cdot 10^{-2}$	(Naito, Hasegawa, Ebe, & Yamamoto, 2004)	Fixed
28	Liver ECF-Pu-Tr	Kupffer Cells	k(14,13)	2.1717	(Reif, et al., 2017)	Fixed

Appendix 1 contains derivations of fixed parameters identified in this table

3.3 Goodness of Fit

The model's expected values will be compared to the actual observed information from the published necropsy data. The goodness of fit for the proposed model will be evaluated via the χ^2 and p-value statistic. The liver and plasma are the focused areas for the variables defined above. Further refinement of the parameters will be attempted when the model provides adequate information to propose an alternative set of parameters.

Akaike Information Criterion (AIC) provides a measure of parsimony or the balance between the goodness-of-fit of a model to a given dataset and model complexity (Aho, Derrryberry, & Peterson, 2014). AIC does not assume there is a known correct or "true" model representing the data, instead it allows for a set of models to be tested relative to each other in order to find the "best" predictive model for the given dataset (Burnham & Anderson, 2002). The general formula for AIC is expressed as:

$$\text{AIC} = -2 \ln (\hat{L}) + 2\text{K} \tag{3-1}$$

$\hat{L}$ represents the maximum value of the likelihood function while K represents the number of optimized parameters in reference to the model under consideration.

AIC may perform poorly when the number of optimized parameters is large compared to the size of the sample data. Therefore, AIC can be manipulated to include an additional bias-correction term when the ratio of sample data, M, to optimized parameters, K, is greater than 40 (Burnham & Anderson, 2002). The corrected AIC is expresses as:

$$\text{AICc} = \text{AIC} + \frac{2K(K+1)}{M-K-1} \tag{3-2}$$

A lower AIC or AICc exemplifies a model that represents the data well while simultaneously being rewarded for having a lower number of optimized parameters. AIC alone cannot be utilized as a measure of the quality of the model. Instead, alternate models are examined and the relative difference in AIC scores is used to select the best model based on the observed data set. AIC and AICc values are reported in this research to facilitate the investigation of future models expanded from this dissertation.

4 Results and Discussion

4.1 Initial Model Performance

Using the initial estimates for each of the parameters, provided in Table 3-2, the model was evaluated for the data set published in Appendix 2. Six of the twenty-eight transfer rates required empirical fitting, Table 4-2, as no *a priori* information was assumed in this initial investigation. The twenty-two fixed transfer rates were chosen to represent *a priori* information based on physiology of the rat, data mining and estimation of published Pu(IV)-citrate rat study information, and proxy rates based on endogenous or xenobiotic kinetics in the rat (Appendix 1 – Initial Model calculation of transfer rates.

Table 4-1 Initial Model Goodness of Fit Statistics

Organ/Tissue	χ^2	df	Critical Value (α=0.05)	p-value	Hypothesis Decision
Liver	6.86	8	15.51	0.55	Fail to reject H_o
Plasma Pu-Citrate	0.774	8	15.51	0.999	Fail to reject H_o
Plasma Pu-Tf	4.04	8	15.51	0.853	Fail to reject H_o
Plasma (total)	3.28	8	15.51	0.916	Fail to reject H_o
Soft Tissue/ECF	0.05	7	14.07	0.999	Fail to reject H_o
Excreta	0.05	7	14.07	0.999	Fail to reject H_o
Skeleton	0.410	8	15.51	0.999	Fail to reject H_o
Model AIC	-139				
AICc	-137				

Examination of the quality of the model is focused on the capability to describe the rat data in terms of directly measured physiological or physiochemical parameters. The primary organ/tissue systems for inspection are Liver, Plasma Pu-Citrate, Plasma Pu-Tf, and Plasma (total). The Soft Tissue/ECF, Excreta, and Skeleton compartments are expected to have good fit statistics based on empirical estimation of the transfer rates from the tissue ECF to the accumulation in the organ system. However, each of the individual ECF compartments were *a priori* informed based on blood flow rates from the plasma to the organ and the resulting fit is a combination of a fixed supply rate and an empirical fit to necropsy data.

Table 4-2 Initial Model - Empirically Solved Transfer Rates

ID	Source Compartment	Target Compartment	Transfer Rate ID	Transfer Rate (hr^{-1})	Std Dev	95% CI	
7	Soft Tissue ECF	Soft tissue	k(3,8)	1.51	$4.67 \cdot 10^{-1}$	0.57	2.44
8	Bone ECF	Bone	k(4,7)	0.709	$1.03 \cdot 10^{-1}$	0.50	0.92
14	Bone	Bone ECF	k(7,4)	$2.56 \cdot 10^{-4}$	$1.87 \cdot 10^{-3}$	-0.003	0.004
17	Soft Tissue	Soft Tissue ECF	k(8,3)	0.115	$3.66 \cdot 10^{-2}$	0.04	0.19
19	GI	Feces	k(10,9)	2.26	$8.43 \cdot 10^{-1}$	0.57	3.95
22	Kidney ECF	Urine	k(12,11)	0.156	$6.33 \cdot 10^{1}$	-0.04	0.35

The initial visual inspection of the plasma data reveals acceptable estimation of the plasma Pu-Cit over the initial period of 48 hours. The model structure provides a visual indication of the rapid exchange of Pu-citrate in plasma among the various organs and the simultaneous competition for binding with vacant transferrin lobes. The observed steep initial slope, Figure 4-1, over the first six hours is thought to be influenced heavily by the vascular delivery of the Pu-citrate to other organ systems. The slower tail is likely a competitive process for the dissociation of Pu from the citrate and subsequent binding to transferrin. The vascular flow contribution appears sufficient to explain this part of model. However, simultaneous analysis of plasma Pu-Tf indicates an insufficient rate of transfer from the Pu-citrate compartments to the Pu-Tf compartments. Pu-citrate is degraded in the plasma within 24 hours and additional analysis of the Pu-citrate and Pu-Tf relationship is warranted.

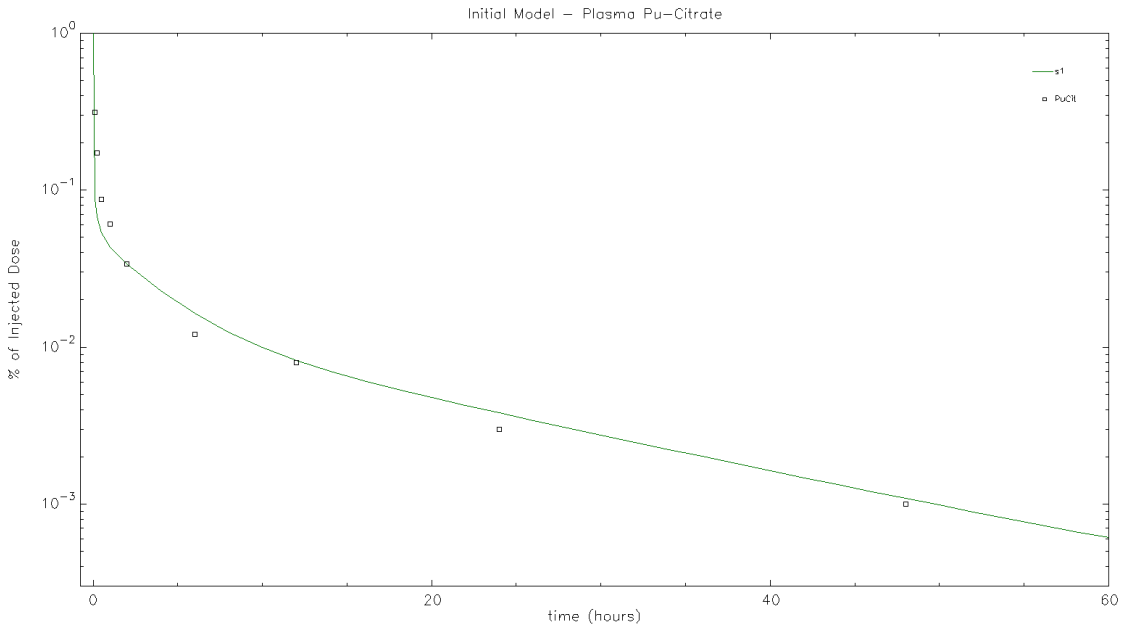

Figure 4-1 Initial Model – Plasma Pu-Citrate model (green line) compared to necropsy data (squares).

The plasma Pu-Tf model indicates a small deviation between the model and the necropsy data, despite still being an acceptable fit. Likewise, the total plasma concentration shows a strong correlation with the plasma Pu-Tf concentration and therefore exhibits a similar fit pattern. The first five data points, up to two hours post injection, are not correlated due to the influence of the Pu-citrate bolus in the total plasma profile. After two hours the Pu-citrate has minimal effect on the total plasma profile, Figure 4-2. Total plasma fitting is not well represented by this set of transfer rates and can likely be improved by selecting alternative transfer rates.

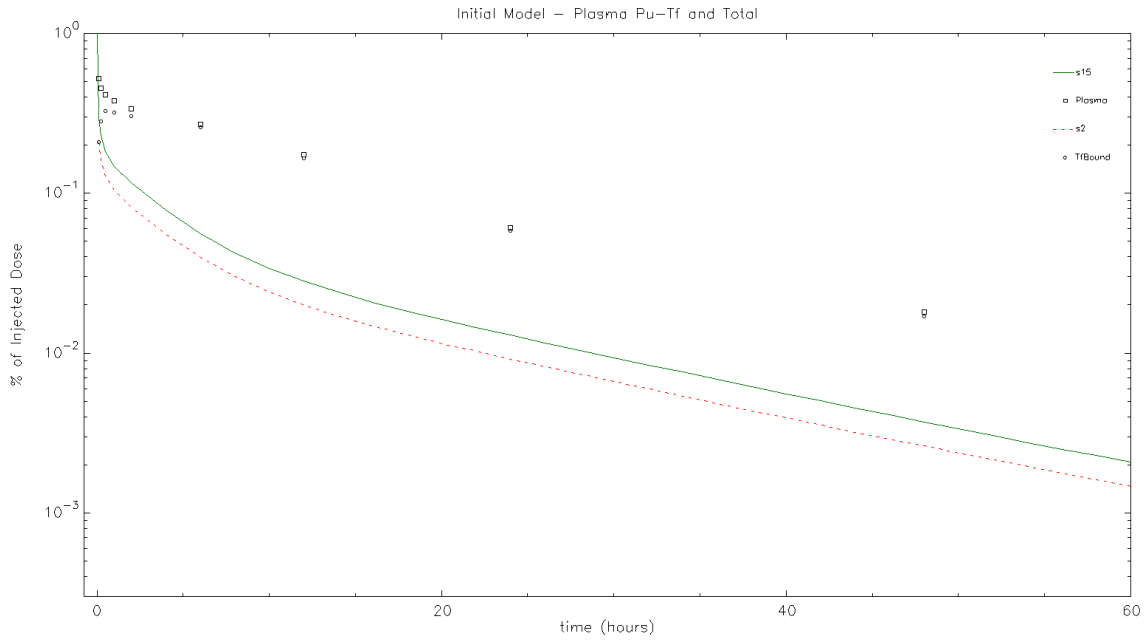

Figure 4-2 Initial Model – Plasma Total (green line, squares) and Plasma Pu-Tf (red dotted line, circles).

Visual inspection of the liver model provides insight on the contribution of hepatocytes and Kupffer cells to the total activity in the liver. The resulting pattern, based on *a priori* estimates of transfer rates, revealed two distinctly different patterns in the influx and efflux from the liver cell population. The hepatocytes show an initial rapid increase in accumulation followed by a rapid and sustained efflux. Kupffer cells exhibit a slower accumulation of Pu and little to no efflux of material over the first 48 hours. The initial model for total liver estimates that hepatocytes control the shape of the kinetic, but the model only marginally follows the observed necropsy data. Inspection of the model's Kupffer cell behavior shows an obviously similar shape to the observed necropsy data, but the magnitude of the model parameters is far below observed values. The combined model provides an acceptable fit to the data and therefore fails to reject the null hypothesis; but improvement in the parameters estimates is likely warranted.

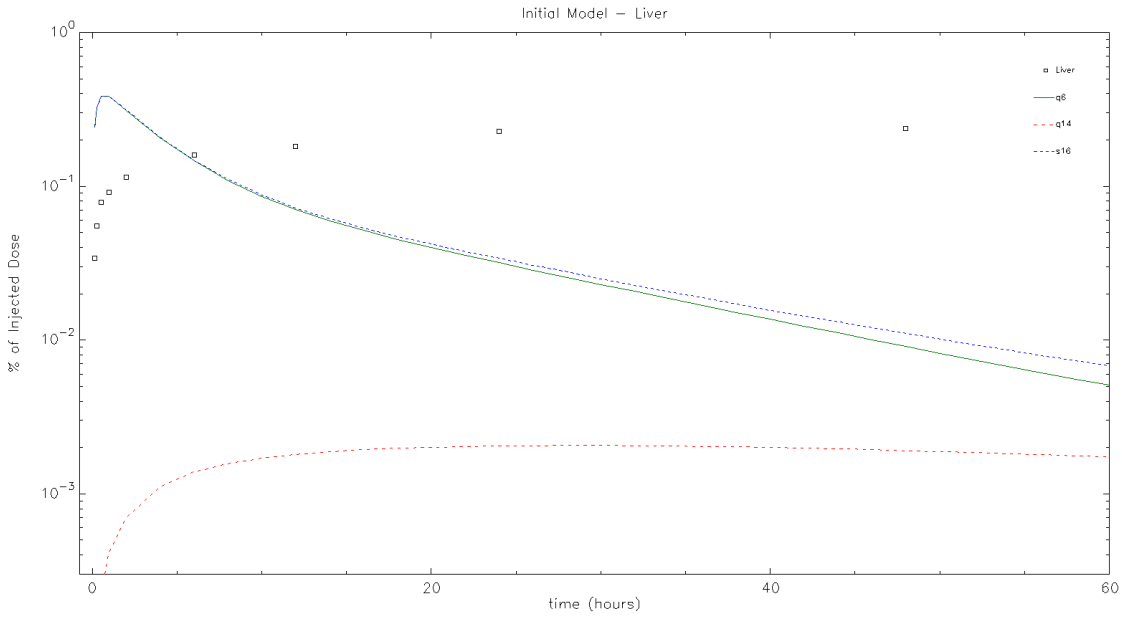

Figure 4-3 Initial Model for Liver (blue dotted line, squares), Hepatocytes (solid green line), and Kupffer Cells (dotted red line).

Simultaneous observation of plasma and liver kinetics reveal similar decreasing slopes which may indicate the correlation between plasma concentration and uptake by hepatocytes from plasma Pu-Tf in the absence of high concentrations of Pu-citrate, especially after the initial six hours post injection.

The soft tissue/ECF, skeleton, and excretion (combined cumulative urine and feces) models all show acceptable fits to the necropsy data with explicit recognition of the empirically derived transfer parameters being directly related to the quality of the fit.

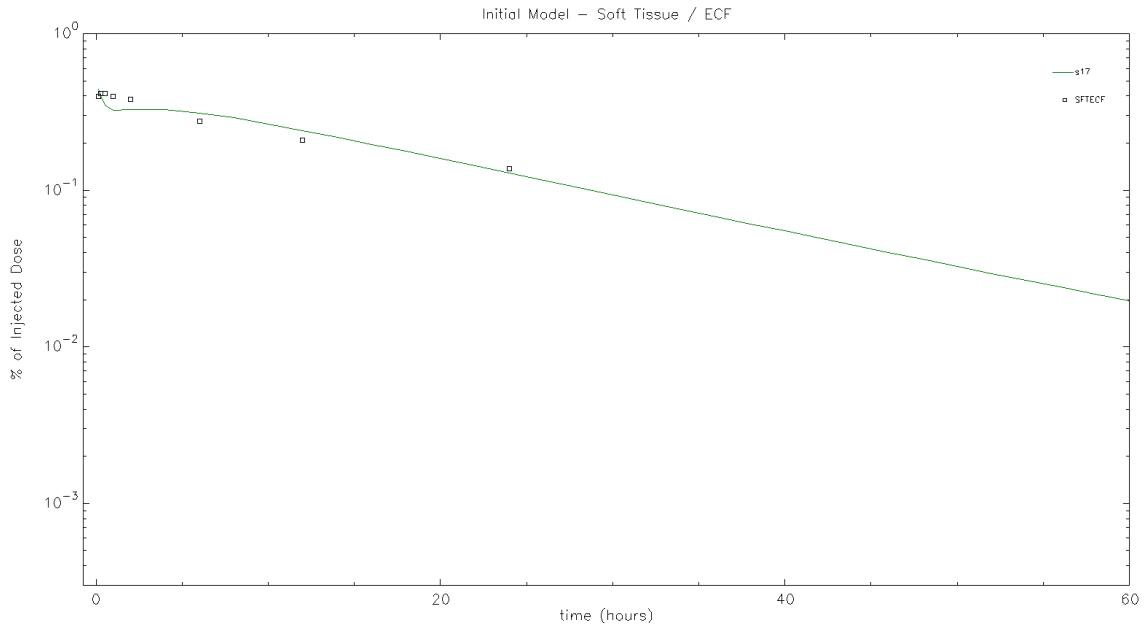

Figure 4-4 Initial Model – Soft Tissue/ECF (solid green line) and combined soft tissue/ECF (squares)

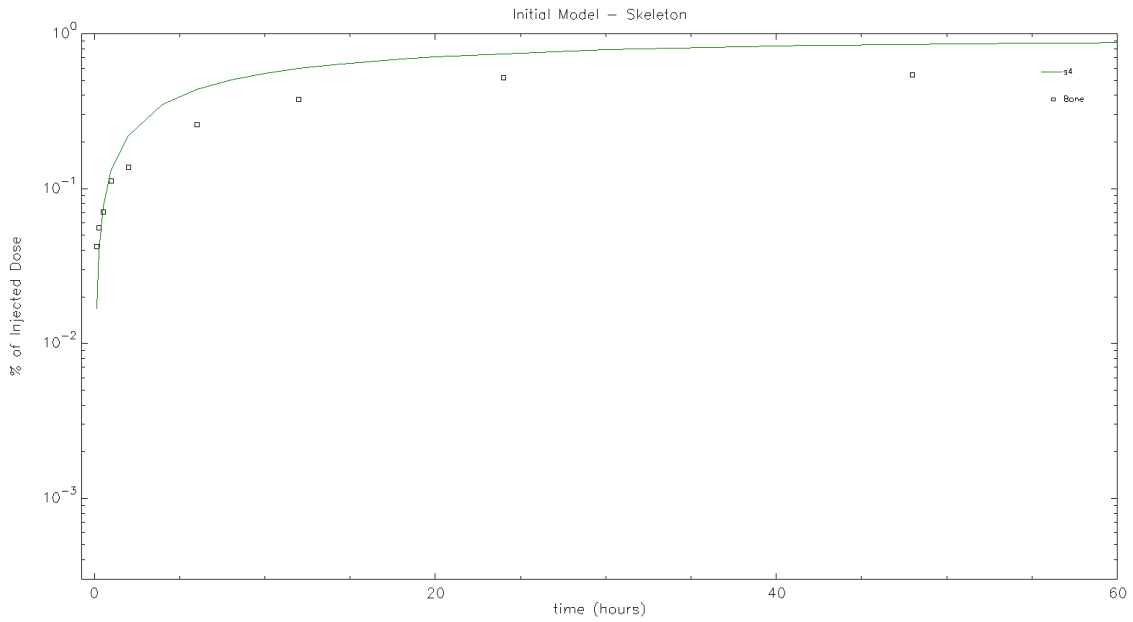

Figure 4-5 Initial Model – Skeleton (solid green line) and skeleton data (squares)

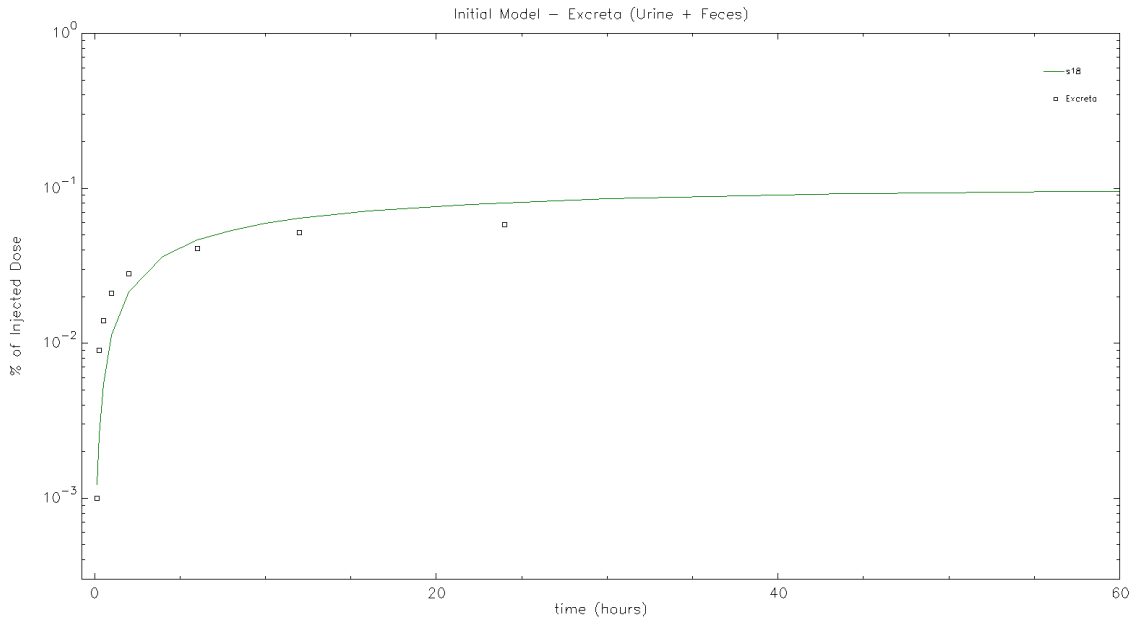

Figure 4-6 Initial Model – Excreta (solid green line) and combined urine and feces data (squares)

Overall, the *a priori* informed model performs adequately for the given data set. The strong performance of this initial model provides enough information to focus efforts on optimizing some of the rates and evaluating the performance and appropriateness of the new parameters.

4.2 Targeted parameter optimization with physiological interpretation

The initial model's performance is acceptable, but inconsistencies in the performance provide an opportunity to further explore the relationship observed in the systems model. Specifically, the shape of the curves associated with hepatocyte and Kuppfer cell compartments lends one to believe that the initial fixed value k(14,13), transfer from liver extra cellular to Kuppfer cells is slower than actually observed in the data. The k(14,13) value was *a priori* estimated based on the assumption that Pu-Tf would behave similarly to Dextran observed from the in vivo kinetic study in Reif, et al.

2017. This assumption appears to limit the absolute performance of the liver system described by the initial model. Conversely, it is observed from Reif, et al. 2017 study that an endogenous material, e.g. CLF, introduced to the liver sinusoidal space is rapidly cleared from the sinusoids and concentrated momentarily in the LSEC/Disse Space.

Simultaneously, the blood plasma Pu-Tf concentration in the model falls below the observed data at all time points. The k(2,1) value can be adjusted to provide an increased amount of Pu-citrate transformating to Pu-Tf. SAAM II will be utilized to empirically estimate the value of the transfer parameters k(14,13) and k(2,1). In this experiement a total of eight transfer rates are adjustable and twenty transfer rates are fixed based on previous *a priori* assumptions. The optimzed results are reported in Table 4-3.

Table 4-3 Optimized transfer parameters for physiological interpretation

	Initial Model	Optimized Model			
	Value (hr^{-1})	Value (hr^{-1})	Std Dev.	95% Conf. Int.	
k(14,13)	2.172	67.61	5.2	57.24	77.99
k(2,1)	$1.069 \cdot 10^{-3}$	261.93	7.2	247.46	276.39

The optimized results are substantially different than the initial model. Given the structure of the systems model it is possible to investigate the physiological merit of the optimzed values.

The transfer rate betweeen plasma Pu-cit and Pu-Tf, k(2,1), indicates that Pu rapidly dissociates from citrate, with a half-life in plasma on the order of 9.5 seconds, after which it is assumed to rapidly bind to transferrin. This rate is extremely fast compared to the transfer rates assumed via vascular transit for movement of Pu-citrate to other compartments outsde the blood plasma. As such, it is expected that Pu-citrate will

be a very limited condition and mostly applicable to the first few hours after exposure via i.v. injection in murine studies. This argument is consistent with the body of knowledge on Pu-citrate behavior *in vivo*.

The transfer rate k(14,13), Pu-Tf liver ECF to Kupffer cells, shows a nearly 31 fold increase compared to the initial model. The 95% confidence interval estimates the rate of transfer from approximately 57 to 78 h^{-1}. The sinusiodal half-life associated with this optimized transfer rate is approximately 37 seconds. This half-life is not consistent with the initial model assumption that Pu-Tf would behave similar to Dextran. Instead, this quick half-life appears to be more consistent with the behavior of an endogenous substance. Reif, et al., 2017 reported a sinusoidal half-life of 1.39 minutes for the endogenous surrogate CLF. A closer examination of the CLF data reveals that endogenous material cleared from the sinusoidal space is concentrated in the LSEC/Disse Space before being transported across hepatocyte membranes. Figure 2.7, Panel C, reports CLF sinusoidal clearance and concentration in the LSEC/Disse Space on a time scale of 24 seconds to 1.4 minutes. Under this new assumption the Pu-Tf is rapidly cleared from the sinusoidal space and concentrated in the LSEC/Disse Space where a majority of the Kupffer cells reside.

The goodness of fit for the revised model was evaluated after it was determined that the optimzed information was physiological plausible. The revised model predictably performs much better than the initial model and it provides information from which further experiments can be conducted.

Table 4-4 Revised Model Goodness of Fit Statistics

Organ/Tissue	χ^2	df	Critical Value (α=0.05)	p-value
Liver	0.002	8	15.51	1
Plasma Pu-Citrate	1.49	8	15.51	0.9926
Plasma Pu-Tf	0.177	8	15.51	0.9999
Plasma (total)	0.115	8	15.51	0.9999
Soft Tissue/ECF	0.111	7	14.07	0.9999
Excreta	0.076	7	14.07	0.9999
Skeleton	0.410	8	15.51	0.9999
Model AIC	-214			
AICc	-212			

The goodness of fit and AIC statistics indicate the revised model is superior to the initial model. However, the quality of the model is validated by the physiological interpretation afforded by the biolgical system model structure. The plasma Pu-Cit compartment under performs in the revised model and as such it provides the opportunity to conduct additional experiments. In the absence of physiological information, results from this type of modeling could lead to the design of *in vitro* experiements to support or refute estimates created in the systems model.

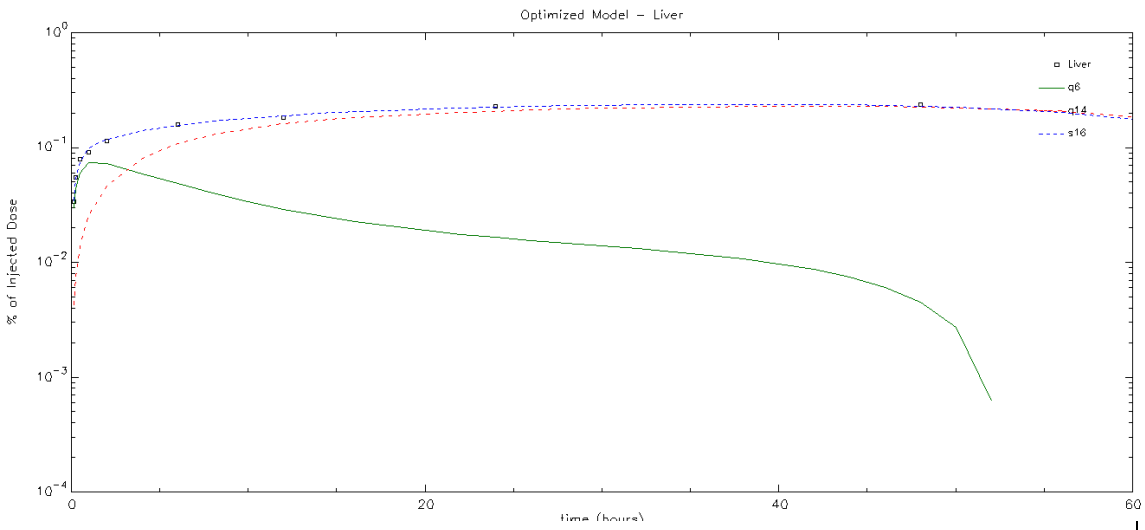

Figure 4-7 Revised Model for Liver (blue dotted line, squares), Hepatocytes (solid green line), and Kupffer Cells (dotted red line).

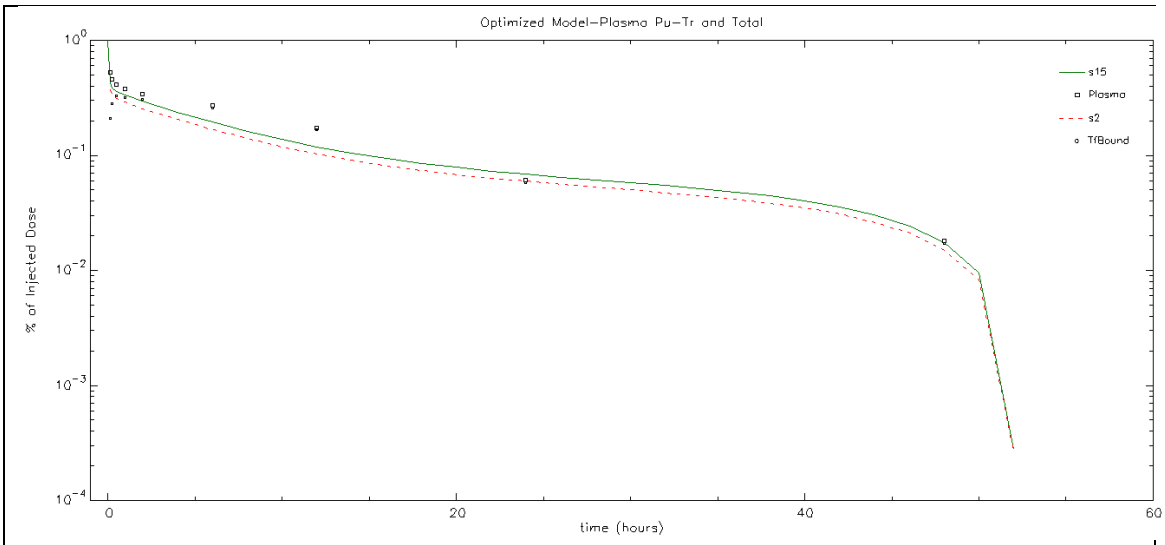

Figure 4-8 Revised Model – Plasma Total (green line, squares) and Plasma Pu-Tf (red dotted line, circles).

5 Conclusion

The goal of this project was to develop a physiologically informed systems level model of the rat for Plutonium and explore the validity of utilizing direct physiological transfer rates to populate the model. The initial model employed 28 transfer rates and only six of the transfer rates were empirically determined. The remaining 22 transfer rates, including all of the blood plasma and liver specific transfer rates, proved that *a priori* physiological rates adequately described the translocation of systemic plutonium over the first 48 hours after a bolus i.v. injection of Pu-citrate.

Validation of the model structure allowed empirical fitting of the two transfer rates that underperformed in the initial model. The revised transfer rates were analyzed to determine their physiological appropriateness before accepting them in the model. The optimized rates indicate that plutonium very rapidly dissociates from citrate and transferrin bound plutonium concentrates in the LSEC/Disse space at a similar rate to other endogenous substances. The proposed model may provide additional hypotheses that can be validated or refuted with *in vitro* experiments.

A priori identification of transfer rates is becoming increasingly important to the internal dosimetry community. This model validates the concept of utilizing physiological information to inform empirical models. An improved understanding of the mechanistic processes that govern the *in vivo* management of plutonium exposures is a vital requirement in the development of effective chelation therapies post exposure. Future physiologically informed models, such as the one proposed in this study, may provide additional cellular level plutonium distribution information which is necessary to improve the micro dosimetry related to charged particle exposure scenarios.

6 References

Aho, K., Derrryberry, D., & Peterson, T. (2014). Model selection for ecologists: the worldviews of AIC and BIC. *Ecology, 95*(3), 631-636.

Allard, B., Kipatsi, H., & Liljenzin, J. O. (1980). Expected species of uranium, neptunium, and plutonium in neutral aqueous solutions. *Journal of Inorganic and Nuclear Chemistry, 42*(7), 1015-1027.

Ansoborlo, E., Prat, O., Moisy, P., Auwer, C. D., Guilbaud, P., Carriere, M., . . . Moulin, V. (2006). Actinide speciation in relation to biological processes. *Biochimie, 88*, 1605-1618.

Aryal, B. P., Gorman-Lewis, D., Paunesku, T., Wilson, R. E., Lai, B., Vogt, S., . . . Jensen, M. P. (2011, October). Plutonium uptake and distribution in mammalian cells: Molecular vs polymeric plutonium. *International journal of radiation biology, 87*(10), 1023-1032.

Ballatori, N. (2002, October). Transport of toxic metals by molecular mimicry. *Environmental Health Persepctives, 110*, 689-694.

Ballou, J. E., & Hess, J. O. (1972, April). BILIARY PLUTONIUM EXCRETION IN THE RAT. *Health Physics*, 369-372.

Barrett, K., Brooks, H., Boitano, S., & Barman, S. (2010). Transport & Metabolic Functions of the Liver. In *Ganong's Review of Medical Physiology* (p. 482). New York: McGraw Hill.

Barton, H. A. (2007, July 16). *Physiologically Based Pharmacokinetic Modeling: An Introduction.* Retrieved February 18, 2020, from U.S. Environmental Protection Agency:

https://cfpub.epa.gov/si/si_public_record_report.cfm?dirEntryId=187288&Lab=NCCT

Basit, H., Tan, M. L., & Webster, D. R. (2019, September 20). Histology, Kupffer Cell. Treasure Island, Florida: StatPearls. Retrieved from https://www.ncbi.nlm.nih.gov/books/NBK493226/

Brissot, P., Wright, T. L., Ma, W.-L., & Weisiger, R. A. (1985). Efficient clearance of non-transferrin-bound iron by rat liver. Implications for hepatic iron loading in iron overload states. *Journal of Clinical Investigation, 76*(4), 1463-1470.

Burnham, K. P., & Anderson, D. R. (2002). *Model Selection and Multimodel Inference - A Practical Information-Theoretic Approach* (Second ed.). New York: Springer.

Carritt, J., Fryxell, R., Kleinschmidt, J., Kleinschmidt, R., Langham, W., San Pietro, A., . . . Schnap, B. (1947). The distribution and excretion of plutonium administered intravenously to the rat. *Journal of Biological Chemistry, 171*(1), 273-283.

Derryberry, D. R. (2014). Appendix B AIC is PRESS! In *Basic Data Analysis for Time Series with R* (pp. 281-283). Wiley.

Durbin, P. W. (1972). Plutonium in Man: A new look at the old data. *Radiobiology of plutonium*, 469-530.

Durbin, P. W., Horovitz, M. W., & Close, E. R. (1972). Plutonium Deposition Kinetics in the Rat. *Health Physics, 22*, 731-741.

Durbin, P. W., Kullgren, B., & Schmidt, C. T. (1972). Circulatory kinetics of intravenously injected 238Pu(IV) citrate and 14C-CaNa3-DTPA in mice: comparison with rat, dog, and reference man. *Health Physics, 72*(2), 222-235.

Fagerholm, U. (2009). Presentation of a modified dispersion model (MDM) for hepatic drug extraction and a new methodology for the prediction of the rate-limiting step in hepatic metabolic clearance. *Xenobiotica, 39*(1), 57-71.

Fraser, R., Cogger, V. C., Dobbs, B., Hamish, J., Warren, A., & Hilmir, S. N. (2012, April). The liver sieve and atherosclerosis. *Pathology, 44*(3), 181-186.

Grube, B. J., Stevens, W., & Atherton, D. R. (1978, January). The retention of plutonium in hepatocytes and sinusoidal lining cells isolated from rat liver. *Radiation Research, 73*(1), 168-179.

Hentze, M. W., Muckenthaler, M. U., & Andrews, N. C. (2004, April 30). Balancing Acts: Molecular Control of Mammalian Iron Metabolism. *Cell, 117*(3), 285-297.

ICRP. (1986). *The Metabolism of Plutonium and Related Elements.* International Commission on Radiological Protection. Oxford: Pergamon Press.

Jensen, M. P., Gorma-Lewis, D., Aryal, B., Paunesku, T., Vogt, S., Rickert, P. G., . . . Soderholm, L. (2011). An iron-dependent and tranferrin-mediated cellular uptake pathway for plutonium. *Nature Chemical Biology, 7*, 560-565.

Joshi, J. G., Sczekan, S. R., & Fleming, J. T. (1989). Ferritin - A general metal detoxicant. *Biological trace elements research, 21*(1), 105-110.

Kilar, F., & Simon, I. (1985, November). The effect of iron binding on the conformation of transferrin. A small angle x-ray scattering study. *Biophysical Journal, 48*(5), 799-802.

Konzen, K. (2014). *Development of a plutonium-DTPA biokinetic model with suggested modification to the plutonium systemic model.* (Doctoral dissertation), Idaho State University.

Kuipers, F., Havinga, R., Booschieter, H., Toorop, G. P., Hindriks, F. R., & Vonk, R. J. (1985). Enterohepatic Circulation in the Rat. *Gastroenterology, 88*(2), 403-411.

Leggett, R. W. (2003). Reliability of the ICRP's dose doefficients for members of the public. III. Plutonium as a case study of uncertainties in the systemic biokinetics of radionuclides. *Radiation Protection Dosimetry, 106*(2), 103-120.

MacDonald, R. A. (1961). "Lifespan" of Liver Cells. *Archives of Internal Medicine, 107*(3), 335-343.

Miller, G., Klumpp, J. A., Poudel, D., Weber, W., Guilmette, R. A., Swanson, J., & Mel, D. R. (2019). Americium Systemic Biokinetic Model for Rats. *Radiation Research, 192*(1), 75-91.

Naito, M., Hasegawa, G., Ebe, Y., & Yamamoto, T. (2004). Differentiation and function of Kupffer cells. *Medical Electron Microscopy, 37*(1), 16-28.

Nunez, M. T. (2010). Regulatory mechanisms of intestinal iron absorption - Uncovering of a fast-response mechanism based on DMT1 and ferroportin endocytosis. *Biofactors, 36*(2), 88-97.

Poisson, J., Lemoinne, S., Boulanger, C., Durand, F., Moreau, R., Valla, D., & Rautou, P.-E. (2017, January). Liver sinusoidal endothelial cells: Physiology and role in liver diseases. *Journal of Hepatology, 66*(1), 212-227.

Popplewell, D. S., Stradling, G. N., & Ham, G. J. (1975, June). The chemical form of Plutonium in Urine. *Radiation Research, 62*(3), 513-519.

Raggatt, L. J., & Partridge, N. C. (2010, August 13). Cellular and Molecular Mechanisms of Bone Remodeling. *Journal Of Biological Chemistry*, 25103-25108. doi:10.1074/jbc.R109.041087

Regoeczi, E., & Chindemi, P. A. (1995). Translocation of different forms of transferrin from blood to bile in the rat. *Hepatology, 21*(4), 1063-1069.

Reif, R., Ghallab, A., Beattie, L., Gunther, G., Kuepfer, L., Kaye, P. M., & Hengstler, J. G. (2017). In vivo imaging of systemic tranport and elimination of xenobiotics and endogeous molecules in mice. *Archives of Toxicology, 91*(3), 1335-1352.

Rosenbaum, S. E. (2017). *Basic Pharmacokinetics and Pharmacodynamics* (Second ed.). (S. E. Rosenbaum, Ed.) Hoboken, New Jersey, USA: John Wiley & Sons, Inc.

Schimmelpfeng, J. (2009). Physiology-based modeling in radiation research: the biokinetics of plutonium. *Radiation Protection Dosimetry, 136*(2), 74-81.

Schumann, K., Elsenhans, B., & Forth, W. (1999). Kinetic analysis of 59Fe movement across the intestinal wall in duodenal rat segments ex vivo. *American Journal of Physiology-Gastrointestinal and Liver Physiology, 276*(2), G431-G440.

Sibille, J.-C., Kondo, H., & Aisen, P. (1988). Interactions between isolated hepatocytes and kupffer cells in iron metabolismL: A possible role for ferritin as an iron carrier protein. *Hepatology, 8*(2), 296-301.

Silva, B., & Faustino, P. (2015, July). An overview of molecular basis of iron metabolism regulation and the associated pathologies. *Biochimica et Biophysica Acta (BBA) - Molecular Basis of Disease, 1852*(7), 1347-1359.

Sluka, J. P., Fu, X., Swat, M., Belmonte, J. M., Cosmanescu, A., Clendenon, S. G., . . . Glazier, J. A. (2016). A Liver-Centric Multiscale Modeling Framework for Xenobiotics. *PLoS ONE, 11*(9), e0162428. doi:10.1371/journal.pone.0162428

Toutain, P. L., & Bousquet-Melou, A. (2004). Volumes of Distribution. *J. vet. Pharmacol. Therap, 27*, 441-453.

Truskey, G. A., Yuan, F., & Katz, D. F. (2009). *Transport Phenomena in Biological Systems* (Second ed.). Saddle River, NJ, USA: Pearson Education, Inc.

Turner, G. A., & Taylor, D. M. (1968). The transport of Plutonium, Americium, and Curium in the blood of rats. *Physics in Medicine & Biology, 13*(4), 538.

U.S. Department of Health and Human Services. (2010). *Toxicological profile for plutonium.* Public Health Service, Agency for Toxic Substance and Disease Registry, Atlanta.

U.S. Environmental Protection Agency (EPA). (2006). *Approaches for the application of physiologically based pharamcokinetic (PBPK) models and supporting data in risk assessment.* Washington DC: National Center for Environmental Assessment.

Welling, P. G. (1995). Difference Between Pharamcokinetics and Toxicokinetics. *Toxicologic Pathology, 23*(2), 143-147.

Ye, M., Swati, N., & Korzekwa, K. (2016). A physiological based pharamcokinetic model to predict the pharamcokinetics of highly protien-bound drugs and the impact of errors in plasma protein binding. *Biopharmaceutics & Drug Distribution, 37*, 123-141. doi:10.1002/bdd.1996

Yuan, D., He, H., Wu, Y., Fan, J., & Cao, Y. (2019, January). Physiologically Based Pharmacokinetic Modeling of Nanoparticles. *Journal of Pharmaceutical Sciences, 108*(1), 58-72.

Appendix 1 – Initial Model calculation of transfer rates

k(1,8) = $\frac{\Sigma\,(\text{Gonad},ST_{ec},\text{Pelt}_{ec},\text{Muscle}_{ec}\rightarrow \text{vPlasma},\text{vPlasma}\rightarrow\text{Lung}_{ec})}{24\cdot 2} = 190\ hr^{-1}$; from Table 2-5

k(2,1) = $\frac{\ln 0.95}{-48\ hr} = 1.069\cdot 10^{-3} hr^{-1}$

95% of the Pu is bound to transferrin within 48 hours. See data table Appendix 2. (Durbin, Horovitz, & Close, Plutonium Deposition Kinetics in the Rat, 1972)

k(2,7) = $\text{Skelton}_{ec} \rightarrow \text{vPlasma} = \frac{228\ d^{-1}}{24\ hrs} = 9.5\ hr^{-1}$; from Table 2-5

k(2,8) = $\frac{\Sigma\,(\text{Gonad},ST_{ec},\text{Pelt}_{ec},\text{Muscle}_{ec}\rightarrow \text{vPlasma},\text{vPlasma}\rightarrow\text{Lung}_{ec})}{24\cdot 2} = 190\ hr^{-1}$; from Table 2-5

k(2,11) = $\text{Skelton}_{ec} \rightarrow \text{vPlasma} = \frac{228\ d^{-1}}{24\ hrs} = 9.5\ hr^{-1}$; from Table 2-5

k(2,13) = $\frac{\Sigma\,(Liver_{ec},\text{Spleen}_{ec}\rightarrow \text{vPlasma})}{24\ hr} = 15{,}295.5\ hr^{-1}$; from Table 2-5

k(3,8) = Empirically Fit

k(4,7) = Empirically Fit

k(5,1) = $\frac{\Sigma\,(\text{aPlasma}\rightarrow Liver_{ec},\text{Spleen}_{ec})}{24\ hr\cdot 2} = 15.4166\ hr^{-1}$; from Table 2-5

k(6,5) = $\frac{\ln 0.67}{-5.55e{-}3\ hr} = 72.1\ hr^{-1}$

67% first pass efficiency clearance of NTBI (Brissot 1985)
Intrinsic transit time of 20 seconds from (Fagerholm 2009)

k(6,13) = $\frac{\ln 0.5}{-0.5695\ hr} = 1.217\ hr^{-1}$

CLF half-life of 34.17 minutes in the hepatocytes (Reif, et al., 2017)

or $= \frac{\ln 0.5}{-0.224333\ hr} = 3.089\ hr^{-1}$

CLF transit half life of 13.46 minutes in LSEC/Disse Space (Reif, et al., 2017)

or $= \frac{\ln 0.5}{-0.0315\ hr} = 22.005\ hr^{-1}$

CLF transit half life of 1.89 minutes in the sinusoids (Reif, et al., 2017)

k(7,1) = $\frac{\text{aPlasma}\rightarrow Liver_{ec}}{24\cdot 2} = 9.4792\ hr^{-1}$; from Table 2-5

k(7,2) = $\frac{\text{aPlasma}\rightarrow Liver_{ec}}{24\cdot 2} = 9.4792\ hr^{-1}$; from Table 2-5

k(7,4) = Empirically Fit

k(8,1) = $\frac{\Sigma\ (\text{aPlasma}\rightarrow \text{Gonad}, ST_{ec}, \text{Pelt}_{ec}, \text{Muscle}_{ec}\ )}{24\cdot 2} = 130.146\ hr^{-1}$; from Table 2-5

k(8,2) = $\frac{\Sigma\ (\text{aPlasma}\rightarrow \text{Gonad}, ST_{ec}, \text{Pelt}_{ec}, \text{Muscle}_{ec}\ )}{24\cdot 2} = 130.146\ hr^{-1}$; from Table 2-5

k(8,3) = Empirically Fit

k(9,6) = $\frac{\ln 0.15}{-1\ hr} =\ 1.897\ hr^{-1}$;

Figure 2-3; 15% of dose collected in duodenum in 1 hour (Ballou 1972)

k(10,9) = Empirically Fit

k(11,1) = $\frac{\text{aPlasma}\rightarrow Kidney_{ec}}{24\cdot 2} = 67.5833\ hr^{-1}$; from Table 2-5

k(11,2) = $\frac{\text{aPlasma}\rightarrow Kidney_{ec}}{24\cdot 2} = 67.5833\ hr^{-1}$; from Table 2-5

k(12,11) = Empirically Fit

k(13,2) = $\frac{\Sigma\ (\ \text{aPlasma}\rightarrow Liver_{ec}, \text{Spleen}_{ec})}{24\ hr\cdot 2} = 15.4166\ hr^{-1}$; from Table 2-5

k(13,5) = $\frac{\ln 0.95}{-48\ hr} =\ 1.069\cdot 10^{-3} hr^{-1}$; See k(2,1) explanation

k(13,6) = $\frac{1}{\tau} = \frac{1}{4800\ hr} = 2.083\cdot 10^{-3} hr^{-1}$

$mean\ life = \tau = 200\ days\ or\ 4800\ hrs$ (MacDonald, 1961)

k(13,9) = $\frac{(\ \text{GI}_{ec}\rightarrow Liver_{ec},)}{24\ hr} = 183.1660\ hr^{-1}$; from Table 2-5

k(13,14) = $\frac{1}{\tau} = \frac{1}{91.2\ hr} = 1.096\cdot 10^{-2} hr^{-1}$

$mean\ life = \tau = 3.8\ days\ or\ 92.1\ hrs$ (Naito, Hasegawa, Ebe, & Yamamoto, 2004)

k(14,13) = $\frac{\ln 0.5}{-0.319166667\ hr} =\ 2.1717\ hr^{-1}$ Dextran transit time in LSEC/Disse Space (Reif, et al., 2017)

Appendix 2 – ^{239}Pu (IV) citrate i.v. injection data for the Rat

Table Appendix 2.0-1 - ^{239}Pu (IV) citrate i.v. injection data for the Rat

(Durbin, Horovitz, & Close, Plutonium Deposition Kinetics in the Rat, 1972)

Table 3. Recalculated distribution of intravenously injected ^{239}Pu(IV) *citrate in the tissues of the young adult female S–D rat.* Data have been corrected for the plasma content of tissues*

Time (hr)	Pu content (% of dose) of compartment					Plasma %/ml	Circulating fractions‡	
	Total plasma	Skeleton	Liver	Excreta†	Soft tissues + extra cellular fluid		Pu_f	Pu_b
	$q_1 + q_2$	q_7	q_5	q_6	$q_3 + q_4 + q_8$			
0.125	52.5	4.2	3.4	0.1	39.8	6.5	0.60	0.40
0.25	45.6	5.6	5.5	0.9	41.5	5.6	0.38	0.62
0.5	41.5	7.1	7.9	1.4	41.6	5.1	0.21	0.79
1	38.0	11.2	9.1	2.1	39.6	4.7	0.16	0.84
2	33.9	13.8	11.4	2.8	38.0	4.2	0.10	0.90
6	27.1	25.8	15.9	4.1	27.5	3.3	0.045	0.955
12	17.4	37.8	18.2	5.2	20.8	2.2	0.045	0.955
24	6.1	51.9	22.7	5.8	13.8	0.75	0.045	0.955
48	1.8	54.5	23.1	—	—	0.22	0.045	0.955

* Sanders et al (12)

Appendix 3 - Initial Model SAAM II Input / Output File

Model Structure:

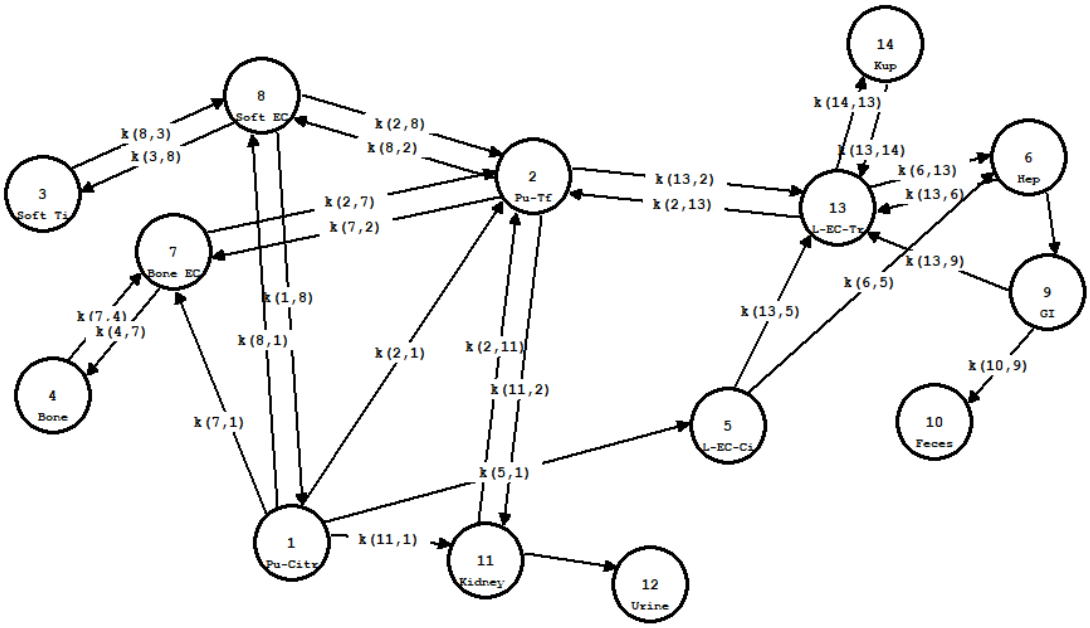

Sample Map:

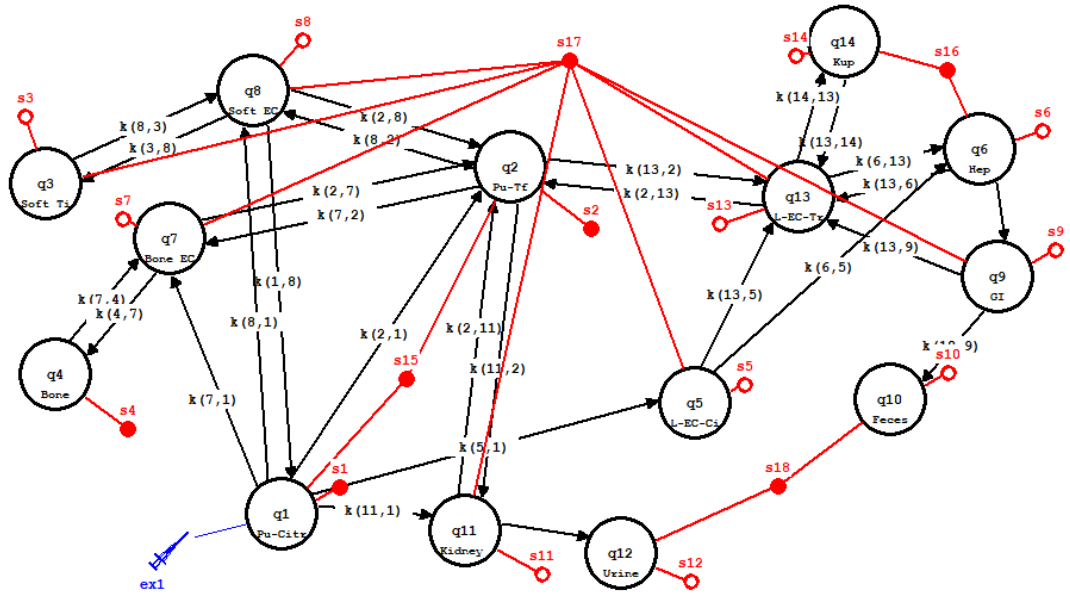

Data Table (dij):

DATA

time	Plasma	PuCit	TfBound	Bone	Liver
0.125	0.525	0.315	0.210	0.042	0.034
0.25	0.456	0.173	0.283	0.056	0.055
0.5	0.415	0.087	0.328	0.071	0.079
1	0.380	0.061	0.319	0.112	0.091
2	0.339	0.034	0.305	0.138	0.114
6	0.271	0.012	0.259	0.258	0.159
12	0.174	0.008	0.166	0.378	0.182
24	0.061	0.003	0.058	0.519	0.227
48	0.018	0.001	0.017	0.545	0.237

END

DATA

time	SFTECF	Excreta
0.125	0.398	0.001
0.25	0.415	0.009
0.5	0.416	0.014
1	0.396	0.021
2	0.38	0.028
6	0.275	0.041
12	0.208	0.052
24	0.138	0.058

END

M= 55 data points (used for AIC)

Exogenous Input:

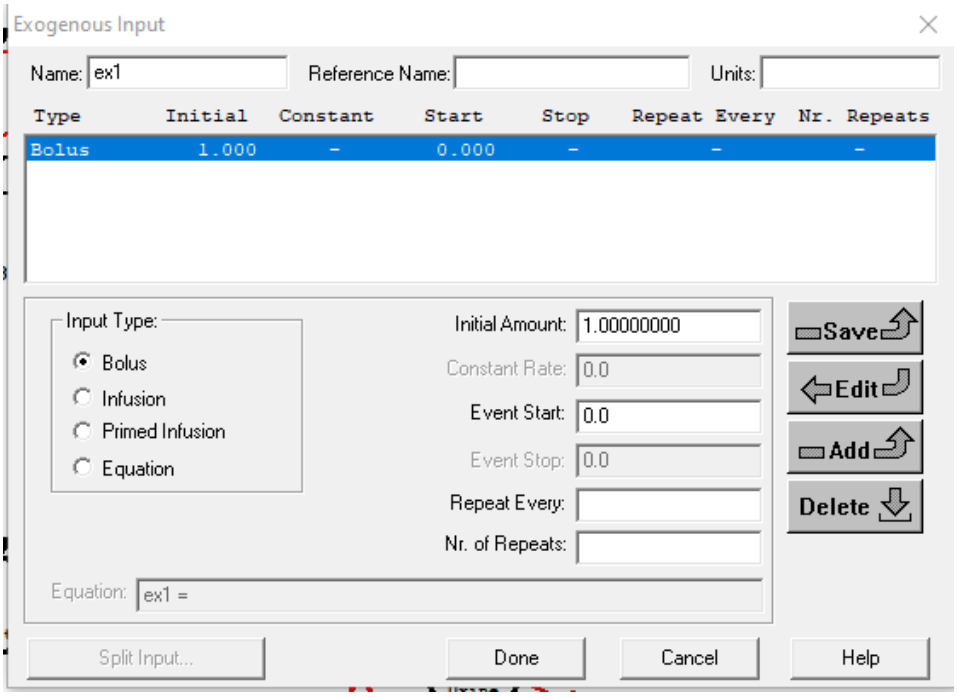

Equations:

```
flux(7,2) = k(7,2) * q2
flux(1,8) = k(1,8) * q8
flux(8,2) = k(8,2) * q2
flux(8,3) = k(8,3) * q3
flux(13,9) = k(13,9) * q9
flux(13,5) = k(13,5) * q5
flux(13,14) = k(13,14) * q14
flux(14,13) = k(14,13) * q13
flux(6,13) = k(6,13) * q13
flux(13,6) = k(13,6) * q6
flux(2,13) = k(2,13) * q13
flux(13,2) = k(13,2) * q2
flux(7,4) = k(7,4) * q4
flux(2,7) = k(2,7) * q7
flux(4,7) = k(4,7) * q7
flux(2,8) = k(2,8) * q8
flux(3,8) = k(3,8) * q8
flux(2,11) = k(2,11) * q11
flux(11,2) = k(11,2) * q2
flux(10,9) = k(10,9) * q9
flux(9,6) = k(9,6) * q6
flux(6,5) = k(6,5) * q5
flux(5,1) = k(5,1) * q1
flux(12,11) = k(12,11) * q11
flux(11,1) = k(11,1) * q1
flux(7,1) = k(7,1) * q1
flux(8,1) = k(8,1) * q1
flux(2,1) = k(2,1) * q1
ex1.bolus = 0.0
ex1.infusion = 0.0
s18 = q10 + q12
s17 = q9 + q13 + q5 + q11 + q8 + q7 + q3
s16 = q6 + q14
s15 = q2 + q1
s14 = q14
s13 = q13
s12 = q12
s11 = q11
s10 = q10
s9 = q9
s8 = q8
s7 = q7
s6 = q6
s5 = q5
s4 = q4
s3 = q3
s2 = q2
s1 = q1
```

Parameter Definitions / Estimates

Parameter/Variable	Value	Std.Dev.	Coef. of Var.	95% Confidence Interval	
k(1,8)	190.00000	** Fixed **	** Fixed **	** Fixed **	** Fixed **
k(2,1)	0.00107	** Fixed **	** Fixed **	** Fixed **	** Fixed **
k(2,7)	9.50000	** Fixed **	** Fixed **	** Fixed **	** Fixed **
k(2,8)	190.00000	** Fixed **	** Fixed **	** Fixed **	** Fixed **
k(2,11)	668.41660	** Fixed **	** Fixed **	** Fixed **	** Fixed **
k(2,13)	15295.00000	** Fixed **	** Fixed **	** Fixed **	** Fixed **
k(3,8)	1.50806	4.66873e-001	3.09586e+001	0.57175	2.44437
k(4,7)	0.70983	1.03186e-001	1.45367e+001	0.50289	0.91677
k(5,1)	15.41660	** Fixed **	** Fixed **	** Fixed **	** Fixed **
k(6,5)	72.10000	** Fixed **	** Fixed **	** Fixed **	** Fixed **
k(6,13)	1.21700	** Fixed **	** Fixed **	** Fixed **	** Fixed **
k(7,1)	9.47920	** Fixed **	** Fixed **	** Fixed **	** Fixed **
k(7,2)	9.47920	** Fixed **	** Fixed **	** Fixed **	** Fixed **
k(7,4)	2.56248e-004	1.87410e-003	7.31361e+002	-0.00350	0.00401
k(8,1)	130.14600	** Fixed **	** Fixed **	** Fixed **	** Fixed **
k(8,2)	130.14600	** Fixed **	** Fixed **	** Fixed **	** Fixed **
k(8,3)	0.11453	3.66243e-002	3.19766e+001	0.04108	0.18798
k(9,6)	1.89700	** Fixed **	** Fixed **	** Fixed **	** Fixed **
k(10,9)	2.26112	8.42776e-001	3.72725e+001	0.57094	3.95130
k(11,1)	67.58330	** Fixed **	** Fixed **	** Fixed **	** Fixed **
k(11,2)	67.58330	** Fixed **	** Fixed **	** Fixed **	** Fixed **
k(12,11)	0.15618	9.88924e-002	6.33190e+001	-0.04215	0.35451
k(13,2)	15.41660	** Fixed **	** Fixed **	** Fixed **	** Fixed **
k(13,5)	0.00107	** Fixed **	** Fixed **	** Fixed **	** Fixed **
k(13,6)	0.00208	** Fixed **	** Fixed **	** Fixed **	** Fixed **
k(13,9)	183.16600	** Fixed **	** Fixed **	** Fixed **	** Fixed **
k(13,14)	0.01096	** Fixed **	** Fixed **	** Fixed **	** Fixed **
k(14,13)	2.17170	** Fixed **	** Fixed **	** Fixed **	** Fixed **

Objective Values

	Objective	Scaled Data Variance
s18 : Excreta	-1.154591e+000	1.980435e+001
s17 : SFTECF	-7.097185e-001	1.916455e+000
s16 : Liver	-1.596683e-001	1.139612e+003
s15 : Plasma	-4.336192e-001	5.097319e+001
s4 : Bone	-6.011973e-001	2.687557e+001
s2 : TfBound	-4.919512e-001	5.485284e+001
s1 : PuCit	-1.231910e+000	1.649507e+001

Total objective	-4.782655e+000	
AIC	-1.259274e+000	
BIC	-1.034345e+000	

***Note: AIC reported in SAAM II is

$$AIC = (L + N_p) / M \quad ;$$

M total number of data points; $M = N_1 + N_2 + \ldots N_j + N_b$

Covariance Matrix:

Covariance Matrix						
	k(3,8)	k(4,7)	k(7,4)	k(8,3)	k(10,9)	k(12,11)
k(3,8)	2.20E-01	2.70E-02	3.30E-04	1.40E-02	1.00E-01	-2.90E-03
k(4,7)	2.70E-02	1.10E-02	1.10E-04	5.90E-04	2.30E-02	-7.50E-04
k(7,4)	3.30E-04	1.10E-04	3.50E-06	2.10E-05	3.00E-04	-1.00E-05
k(8,3)	1.40E-02	5.90E-04	2.10E-05	1.30E-03	2.00E-03	-2.10E-05
k(10,9)	1.00E-01	2.30E-02	3.00E-04	2.00E-03	7.10E-01	-5.90E-02
k(12,11)	-2.90E-03	-7.50E-04	-1.00E-05	-2.10E-05	-5.90E-02	9.80E-03

Correlation Matrix:

Correlation Matrix						
	k(3,8)	k(4,7)	k(7,4)	k(8,3)	k(10,9)	k(12,11)
k(3,8)	1.00000	0.56735	0.37206	0.80898	0.25490	-0.06274
k(4,7)	0.56735	1.00000	0.56983	0.15600	0.26907	-0.07368
k(7,4)	0.37206	0.56983	1.00000	0.31107	0.18937	-0.05456
k(8,3)	0.80898	0.15600	0.31107	1.00000	0.06577	-0.00575
k(10,9)	0.25490	0.26907	0.18937	0.06577	1.00000	-0.70242
k(12,11)	-0.06274	-0.07368	-0.05456	-0.00575	-0.70242	1.00000